IDEA League

Master of Science in Applied Geophysics

Research Thesis

Pressure and Velocity Fields Retrieval Based on a New Normalization Option and 1D Model-Free Primaries Retrieval from Marine Data

New Marchenko-type Equations with Two-Way Wavefields at the Receiver Level

Jiahui Kang

August 10, 2018

Pressure and Velocity Fields Retrieval Based on a New Normalization Option and 1D Model-Free Primaries Retrieval from Marine Data

New Marchenko-type Equations with Two-Way Wavefields at the Receiver Level

Master of Science Thesis

for the degree of Master of Science in Applied Geophysics at

Delft University of Technology

ETH Zürich

RWTH Aachen University

by

Jiahui Kang

August 10, 2018

Department of Geoscience & Engineering · Delft University of Technology
Department of Earth Sciences · ETH Zürich
Faculty of Georesources and Material Engineering · RWTH Aachen University

Delft University of Technology

Printed in The Netherlands

IDEA LEAGUE
JOINT MASTER'S IN APPLIED GEOPHYSICS

Delft University of Technology, The Netherlands
ETH Zürich, Switzerland
RWTH Aachen, Germany

Dated: *August 10, 2018*

Supervisor(s):

Prof. Dr. Ir. Evert Slob

Lele Zhang

Committee Members:

Prof. Dr. Ir. Evert Slob

Prof. Dr. Florian Wellmann

Lele Zhang

Abstract

The Marchenko method is being developed to compute redatuming operators from the reflection response based on a new normalization option at the data level. These operators can be used to retrieve the two-way focusing functions in terms of pressure and velocity, respectively, without effects from the ghost, and free-surface and internal multiples. To compute these operators an estimate of the first arrival of the redatuming operator is required. This can be done using the same model as is used for traditional migration. We then propose to delay the need for such a model and remove free-surface and internal multiples in one step while retaining the primary reflections at the original two-way traveltime. We modify the amplitude by removing the transmission effects at both sides of the equations. The resulting data becomes full focusing functions in terms of pressure and velocity at two-way traveltime, respectively. New datasets can then be generated by picking the value at each focusing level and storing it which are free of the ghost effects, free surface and internal multiples.

Acknowledgements

First of all, I want to thank Prof. Slob who has been instructing me patiently. His knowledge of wave theory helped me a lot since the work behind this thesis really takes a solid understanding of the corresponding theory which makes it a bit hard to start with. He always encourages me to explore the scheme independently rather than doing what is told which definitely of long-term effect for me. I also want to express my heartfelt thanks to Lele Zhang for helping me to understand the projection scheme. He was always ready to help me regarding both theory and implementation of the projected Marchenko scheme. I want to thank Bingkun Yang who worked with me last year when I started to learn about the Marchenko scheme. He helped me to implement the LSQR scheme which could solve for focusing functions considering the presence of free-surface. Great thanks to Jan Thorbecke and Joost van der Neut who developed an impressive algorithm for implementing the Marchenko scheme in 2D case. The algorithm together with the manual was so helpful for me to better understand the implementation of Marchenko scheme in a much more complex case. Special thanks to my friends who have been studying with me for the past six months.

Delft University of Technology
August 10, 2018

Jiahui Kang

Table of Contents

List of Figures

List of Tables

Acronyms

DUT Delft University of Technology

ETH Swiss Federal Institute of Technology

RWTH Aachen University

August 10, 2018

Chapter 1

Introduction

In seismic data processing, finding a proper scheme to handle data with the ghost effects, free surface and internal multiples is a sustained challenge. For marine data, sources and receivers are located in the water column. This causes not only internal multiples but also significant free-surface multiples with strong reflections at the air-water 'free surface' as well as the ghost effects.

1-1 Development of Marchenko redatuming scheme with differently normalized wavefields

Lots of algorithms have been developed on internal multiples elimination, for example, in [Weglein et al., 1997, Jakubowicz, 2005, Kelamis et al., 2006, Fomel, 2009, King et al., 2013, Cypriano et al., 2015]. Among them, the inverse scattering method is a traditional method and it starts with a reference medium which agrees with the actual medium at and above the measured surface and estimates the internal multiples at once. The computation of inverse scattering series requires accurate seismic data with a broad frequency bandwidth such as accurate source signature. Otherwise, a proper filter will be needed [Matson et al., 1999].
Recently, the work of [Rose, 2002] shows that by solving a Marchenko equation, we can focus a 1D wavefield in an unknown medium. This drove the idea of using the Marchenko equation to retrieve a virtual seismic velocity profile. Then based on the wavefield focusing idea, in [Broggini et al., 2012] they illustrated in 1D that a vertical seismic profiling (VSP) Green's function was obtained with a virtual source inside the medium and a receiver above the subsurface by focusing the field inside an unknown medium. [Wapenaar et al., 2013] shows that a 3D Marchenko equation can be derived from which focusing functions can be computed that in turn can be used to compute the VSP Green's function and the estimate of the first arrival of the downgoing focusing function can be made when a macro-velocity model is available. Following this work, [Broggini et al., 2014] then proposed the data-driven wavefield focusing method to retrieve the Green's function. [Slob et al., 2014] derived the

Marchenko equation from reciprocity as two coupled equations for the up- and downgoing parts simultaneously. The importance is that only one Marchenko-type equation should be solved instead of two to find the up- and downgoing parts of the focusing functions of the VSP Green's functions. The odd and the even iterates of the combined scheme also give the up- and downgoing parts, see [Thorbecke et al., 2017]. It shows that an artifact-free image with true amplitude can be made not only with the Green's function but also with the focusing function. In [Wapenaar et al., 2014a], they discussed the Green's function retrieval in terms of acoustic flux and pressure. In [Wapenaar et al., 2014b], they gave the rigorous 3D derivation with pressure-normalized data and showed how an artifact-free image can be made. In the work of [Singh et al., 2015], they included free surface multiples for land data and used flux-normalization. With the coupled Marchenko equations, up- and downgoing Green's functions are retrieved at an arbitrary depth level and imaging can be done afterward. In [Singh et al., 2017], they discussed the scheme with pressure-normalized wavefields. To deal with the complex overburden problem with Marchenko scheme, the revised Marchenko equations considering the different source and receiver depth levels were developed for marine data in [Slob and Wapenaar, 2017, Ravasi, 2017]. They used pressure in the reference medium and velocity in the actual medium at the receiver level and the reverse choices were made at the focusing level with wavefield decomposition. In [Zhang et al., 2018a], they revised the redatuming Marchenko equation with a new truncation operator and they used a time-reversed version of the standard wavefields-extrapolation operator as the initial estimate to improve the reverse time migration imaging. It is important to realize that in the existing literature, the one-way wavefields are represented in different ways and the space-time behavior of retrieved focusing functions as well as the focusing condition are treated differently.
In our scheme, we play with different versions of reciprocity theorems based on a new normalization option. We keep the two-way wavefields at the receiver level and normalize the fields at the focusing level so that we can retrieve the true two-way focusing wavefields without decomposing the received data. With different choices of normalization at the focusing level and the focusing conditions, we obtain different pressure and velocity related two-way focusing wavefields.

1-2 Marchenko equations at the receiver level

The work in [van der Neut and Wapenaar, 2016] shows that the Marchenko equation can be modified to keep the results in two-way travel time with flux-normalized wavefields that are decomposed in up- and downgoing components such that the upgoing part is the reflection response. They rewrote the Marchenko equation by applying a projection operator. This scheme removes the unknown initial estimate as in [Slob et al., 2014] so that it doesn't need a macro-velocity model but it requires a two-way traveltime surface of a horizon in the subsurface. In [Zhang et al., 2018b], they achieved the free-surface and internal multiples elimination and transmission losses compensation without the need of a horizon. Their scheme works for any time point but with assumptions that the source wavelet can be well recovered and the evanescent waves, as well as refractions, are absent.
Here we revise the equations with new normalization option in the 1D situation to keep the results in two-way travel time based on the redatuming scheme so that our whole scheme becomes a model-free scheme. We tested our scheme with marine seismic data including free-surface multiples and borehole seismic data and for zero and oblique angles of incidence.

Chapter 2

Classical Marchenko-type Equations for One-way Wavefields

Marchenko imaging of marine seismic data and land data using the vertical component of velocity separated in up- and downgoing components with the focusing functions at the receiver level as the up- and downgoing components of acoustic pressure are presented in [Slob and Wapenaar, 2017, Ravasi, 2017]. They also adapted the scheme to account for data with different source and receiver depth levels, for example, marine seismic data with free-surface, borehole seismic data and so on. In the following, I will start with the decomposition methods and then present the basic derivation of classical Marchenko scheme for land data as well as marine data basically in terms of acoustic pressure.

2-1 Wave equation

The wave equation is the basis of Marchenko-type equations since it describes the mechanism of the wavefields' propagation inside the medium. To obtain the acoustic two-way wave equation the solution of which is the reflection response, we start with the linear differential equations of Newton's law and Hooke's law given by [Wapenaar and Berkhout, 1989]

$$\nabla \cdot \mathbf{v} + \kappa \frac{\partial p}{\partial t} = q, \tag{2-1}$$

$$\nabla p + \rho \frac{\partial \mathbf{v}}{\partial t} = \mathbf{f}, \tag{2-2}$$

where $\mathbf{v}$ is the particle velocity, p is the acoustic pressure, ρ is the density, κ is defined as the compressibility and q and $\mathbf{f}$ represents the monopole injection rate and the volume density of external force, respectively. After combining Eq. (2-1) and Eq. (2-2) to eliminate the particle velocity $\mathbf{v}$, we obtain the wave equation for the acoustic pressure p:

$$\rho \nabla \cdot (\frac{1}{\rho} \nabla p) - \frac{1}{c^2} \frac{\partial^2 p}{\partial t^2} = -s, \tag{2-3}$$

where $c = \sqrt{\frac{1}{\kappa\rho}}$ which represents the wave propagation velocity and s includes a source distribution in terms of volume injection rate q and the volume density of force $\mathbf{f}$. The relation between particle velocity and acoustic pressure in frequency domain is $\hat{\mathbf{v}} = -\frac{1}{j\omega\rho}\nabla\hat{p}$.
Provided that an impulse source is excited at $\mathbf{x}'_r$ at level $\partial\mathbb{D}_r$ in the actual medium, then the Green's function $G(\mathbf{x}_r, \mathbf{x}'_r, t)$ is defined as the response to an impulsive point source of volume injection rate of the subsurface received at $\mathbf{x}_r$. It fulfills the wave equation [Wapenaar and Berkhout, 1989, Wapenaar et al., 2014b]

$$\rho(\mathbf{x})\nabla\cdot(\frac{1}{\rho(\mathbf{x})}\nabla G) - \frac{1}{c(\mathbf{x})^2}\frac{\partial^2 G}{\partial t^2} = -\rho(\mathbf{x})\delta(\mathbf{x}-\mathbf{x}'_r)\frac{\partial\delta(t)}{\partial t}, \tag{2-4}$$

where $c(\mathbf{x})$ and $\rho(\mathbf{x})$ are the position-related propagation velocity and mass density.
The Green's function only contains information of the targeted subsurface such as primary reflections and internal multiples. It can be decomposed into downgoing field and upgoing field at the receiver level in a way that $G(\mathbf{x}_r, \mathbf{x}'_r, t) = G^+(\mathbf{x}_i, \mathbf{x}'_r, t) + G^-(\mathbf{x}_i, \mathbf{x}'_r, t)$ [Wapenaar and Berkhout, 1989, Wapenaar et al., 2014b] in terms of acoustic pressure to derive the one-way Marchenko equations. In Figure 2-1, several possible paths are presented as an example. Notice that even though multiples are not presented, they are not negligible and contribute to the imaging procedure and the direct downgoing Green's function is also shown in the figure.

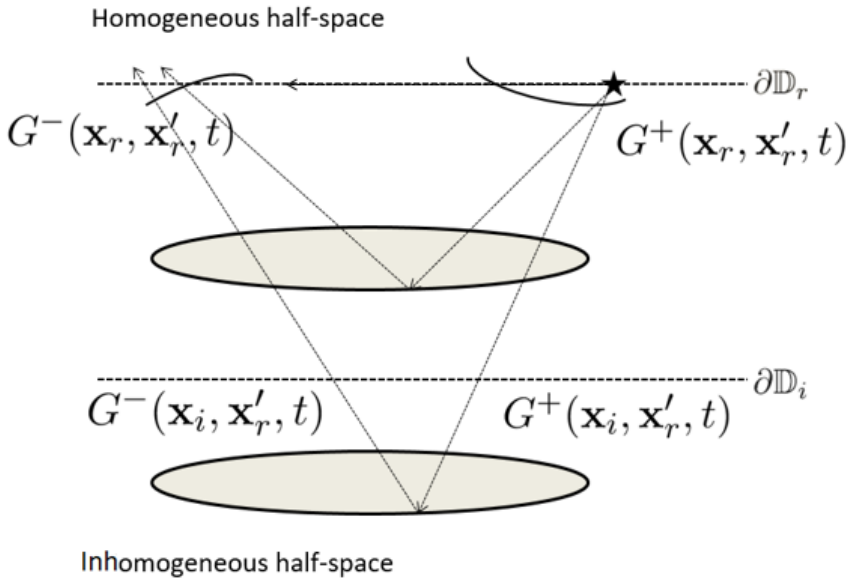

Figure 2-1: Downgoing and upgoing Green's wavefields in the actual medium

Inside the medium, there is no external volume force or mass injection acting. The field vector can be decomposed into up- and downgoing wavefields p^+ and p^- with the relationship given by [Ursin, 1983, P. Corones et al., 1983, Claerbout, 1985, Fishman, 1987, Wapenaar and Berkhout, 1989, Fishman, 1993, Wapenaar, 1998, Wapenaar et al., 2001]

$$\begin{bmatrix} p \\ v_z \end{bmatrix} = \begin{bmatrix} \mathcal{L}_1 & \mathcal{L}_1 \\ \mathcal{L}_2 & -\mathcal{L}_2 \end{bmatrix} \begin{bmatrix} p^+ \\ p^- \end{bmatrix}, \tag{2-5}$$

where $\mathcal{L}_1$ and $\mathcal{L}_2$ are defined as pseudo-differential operators. By keeping $\mathcal{L}_2$ and $-\mathcal{L}_2$ for the relation between two-way vertical particle velocity and normalized one-way wavefields, the up- and downgoing wavefields are always pressure-like with respect to reflection and $R = \frac{p^-}{p^+}$ where R is the reflection response. The choice of the whole matrix $\mathcal{L}$ is dependent on the choice of normalization methods of the one-way wavefields as indicated below. We will continue with the different choices and discuss at which depth level decomposition should be applied in next chapter.

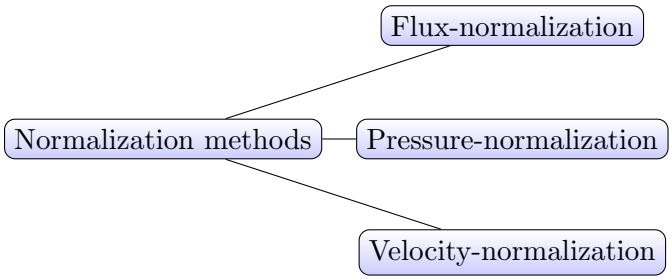

Figure 2-2: Normalization Options

2-2 3D artifact-free Marchenko imaging

Here we briefly introduce the classical Marchenko imaging theory in terms of acoustic pressure to provide readers with an insight into Marchenko imaging. The 3D Marchenko imaging in [Wapenaar et al., 2014b] is aimed at making an artifact-free image which requires up- and downgoing parts of a Green's function at a depth level. The Green's functions can be obtained from the Green's function representation with the need for knowledge of reflection response and the focusing functions. The focusing functions can be computed from the reflection response using the Marchenko-type equations. The retrieved Green's function includes not only primary reflections but also internal multiples.
In the reference configuration, we take the medium between depth levels $\partial\mathbb{D}_i$ and $\partial\mathbb{D}_r$ equal to the actual medium, whereas below $\partial\mathbb{D}_i$ and above $\partial\mathbb{D}_r$ the medium is homogeneous as indicated in Figure 2-3. Similar to the decomposition of G in the sense of pressure-normalization, the acoustic pressure related focusing function can be written as the superposition of downgoing and upgoing fields: $f_1(\mathbf{x}, \mathbf{x}_i, t) = f_1^-(\mathbf{x}, \mathbf{x}_i, t) + f_1^+(\mathbf{x}, \mathbf{x}_i, t)$ [Wapenaar et al., 2014b].

Since it is defined to focus at $\mathbf{x}_i$, we can write the focusing condition as [Wapenaar et al., 2014b]

$$\partial_z f_1^+(\mathbf{x}, \mathbf{x}_i, t)|_{x_z = x_{z,i}} = -\frac{1}{2}\rho(\mathbf{x}_i)\delta(\mathbf{x}_H - \mathbf{x}_{H,i})\frac{\partial\delta(t)}{\partial t}, \tag{2-6}$$

$$\partial_z f_1^-(\mathbf{x}, \mathbf{x}_i, t)|_{x_z = x_{z,i}} = 0. \tag{2-7}$$

Note that the focusing functions in this case are pressure fields. Eq. (2-6) and Eq. (2-7) means that the vertical particle velocity focus at $\mathbf{x}_i$. We can understand $f_1^\pm$ from a holistic

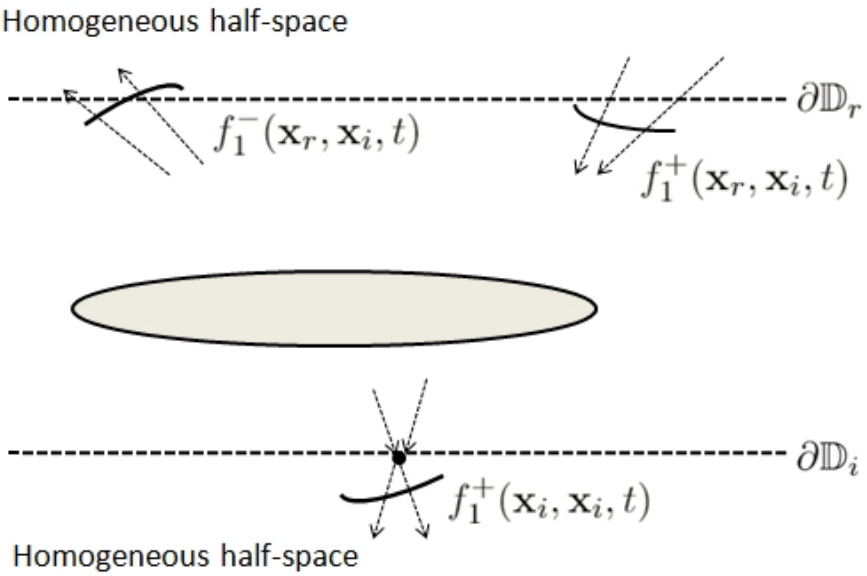

Figure 2-3: Downgoing and upgoing focusing functions in the reference medium

view that to focus acoustic wavefield at a certain level, we have to send in a wavefield f_1^+ with the amplitude of the inverse of the transmission response at $\partial\mathbb{D}_i$ to an impulsive point source of volume injection rate. And the upgoing focusing function is interpreted as the reflection response of the downgoing wavefield, see Figure 2-4. This is explained in detail in [Slob et al., 2014].

For the sake of clearness, we define two scenarios in Figure 2-1 and Figure 2-3 as state B and state A, respectively. To begin with, the reciprocity theorems of the time-convolution and time-correlation types for pressure-normalized one-way wavefields can be expressed as [Slob and Wapenaar, 2017]

$$\begin{aligned}&\int_{\partial\mathbb{D}_r}[\hat{p}_A^+(\mathbf{x}_r)\hat{v}_{z,B}^-(\mathbf{x}_r)+\hat{p}_A^-(\mathbf{x}_r)\hat{v}_{z,B}^+(\mathbf{x}_r)]d\mathbf{x}_r\\&=-\int_{\partial\mathbb{D}_i}[\hat{v}_{z,A}^+(\mathbf{x}_i)\hat{p}_B^-(\mathbf{x}_i)+\hat{v}_{z,A}^-(\mathbf{x}_i)\hat{p}_B^+(\mathbf{x}_i)]d\mathbf{x}_i,\end{aligned}\tag{2-8}$$

$$\begin{aligned}&\int_{\partial\mathbb{D}_r}[(\hat{p}_A^+(\mathbf{x}_r))^*\hat{v}_{z,B}^-(\mathbf{x}_r)+(\hat{p}_A^-(\mathbf{x}_r))^*\hat{v}_{z,B}^+(\mathbf{x}_r)]d\mathbf{x}_r\\&=\int_{\partial\mathbb{D}_i}[(\hat{v}_{z,A}^+(\mathbf{x}_i))^*\hat{p}_B^-(\mathbf{x}_i)+(\hat{v}_{z,A}^-(\mathbf{x}_i))^*\hat{p}_B^+(\mathbf{x}_i)]d\mathbf{x}_i,\end{aligned}\tag{2-9}$$

where in Eq. (2-9) we assume that the evanescent waves are neglected at both focusing and data levels. The reason is introduced in Appendix A.

As indicated above, the acoustic pressure related focusing wavefield $\hat{f}_1$ represents $\hat{p}_A$ while the Green's wavefield $\hat{G}$ in terms of acoustic pressure represents $\hat{p}_B$ which can be expressed as

$$\hat{p}_B=\hat{G}=\hat{G}^+ + \hat{G}^-,\tag{2-10}$$

$$\hat{v}_{z,B}=-\frac{1}{j\omega\rho}\partial_z\hat{G}=-\frac{1}{j\omega\rho}(\partial_z\hat{G}^+ + \partial_z\hat{G}^-),\tag{2-11}$$

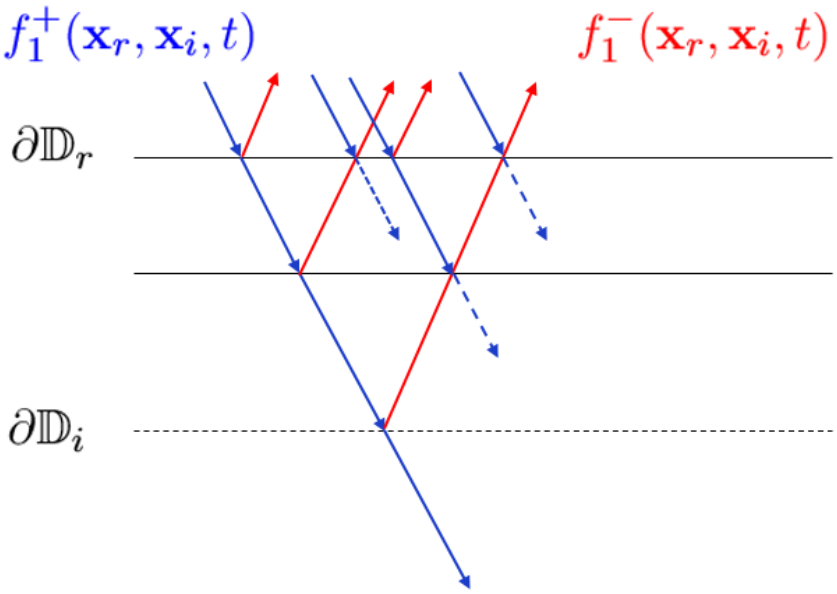

Figure 2-4: Illustration of up- (red) and downgoing (blue) focusing wavefields

$$\hat{p}_A = \hat{f}_1 = \hat{f}_1^+ + \hat{f}_1^-, \tag{2-12}$$

$$\hat{v}_{z,A} = -\frac{1}{j\omega\rho}\partial_z \hat{f}_1 = -\frac{1}{j\omega\rho}(\partial_z \hat{f}_1^+ + \partial_z \hat{f}_1^-), \tag{2-13}$$

We can substitute the focusing condition indicated in Eq. (2-6) and Eq. (2-7) into Eq. (2-8) and Eq. (2-9). The relations between upgoing and downgoing Green's functions $G^{\pm}(\mathbf{x}_i, \mathbf{x}'_r, t)$ and focusing functions $f_1^{\pm}(\mathbf{x}_r, \mathbf{x}_i, t)$ are then given as [Wapenaar et al., 2014b]

$$G^-(\mathbf{x}_i, \mathbf{x}'_r, t) = \int_{\partial\mathbb{D}_r} d\mathbf{x}_r \int_{-\infty}^{t} R^{\cup}(\mathbf{x}_r, \mathbf{x}'_r, t-t') f_1^+(\mathbf{x}_r, \mathbf{x}_i, t') dt' - f_1^-(\mathbf{x}_r, \mathbf{x}_i, t), \tag{2-14}$$

$$G^+(\mathbf{x}_i, \mathbf{x}'_r, t) = -\int_{\partial\mathbb{D}_r} d\mathbf{x}_r \int_{-\infty}^{t} R^{\cup}(\mathbf{x}_r, \mathbf{x}'_r, t-t') f_1^-(\mathbf{x}_r, \mathbf{x}_i, -t') dt' + f_1^+(\mathbf{x}_r, \mathbf{x}_i, -t), \tag{2-15}$$

where $R^{\cup}(\mathbf{x}_r, \mathbf{x}'_r, t-t')$ is the reflection response without free-surface multiples of the subsurface with the relation given by

$$\partial_z G^-(\mathbf{x}_r, \mathbf{x}'_r, t)|_{x_{z,r}=x'_{z,r}} = \frac{1}{2}\rho \frac{\partial R^{\cup}(\mathbf{x}_r, \mathbf{x}'_r, t)}{\partial t}, \tag{2-16}$$

and the expression for $G^+(\mathbf{x}_r, \mathbf{x}'_r, \omega)$ is

$$\partial_z G^+(\mathbf{x}_r, \mathbf{x}'_r, t)|_{x_{z,r}=x'_{z,r}} = -\frac{1}{2}\rho\delta(\mathbf{x}_{H,r} - \mathbf{x}'_{H,r}) \frac{\partial\delta(t)}{\partial t}. \tag{2-17}$$

Eq. (2-14) and Eq. (2-15) can be estimated with a time window $t < t_d(\mathbf{x}_i, \mathbf{x}_r)$ and then we have [Wapenaar et al., 2014b]

$$0 = \int_{\partial\mathbb{D}_r} d\mathbf{x} \int_{-\infty}^{t_d} R^{\cup}(\mathbf{x}_r, \mathbf{x}'_r, t-t') f_1^+(\mathbf{x}_r, \mathbf{x}_i, t') dt' - f_1^-(\mathbf{x}_r, \mathbf{x}_i, t), \tag{2-18}$$

$$0 = -\int_{\partial\mathbb{D}_r} d\mathbf{x} \int_{-\infty}^{t_d} R^{\cup}(\mathbf{x}_r, \mathbf{x}'_r, t-t') f_1^-(\mathbf{x}_r, \mathbf{x}_i, -t') dt' + f_1^+(\mathbf{x}_r, \mathbf{x}_i, -t). \tag{2-19}$$

This is because the Green's functions $G^{\pm}(\mathbf{x}_i, \mathbf{x}'_r, t)$ are casual and only appear at and after the direct arrivals from $\mathbf{x}'_r$ to $\mathbf{x}_i$. Eq. (2-18) and Eq. (2-19) are known as the Marchenko integral equations which can be solved with an iterative scheme modified from the 1D case in [Slob et al., 2014] to obtain $f_1^{\pm}(\mathbf{x}_r, \mathbf{x}_i, t)$ with the estimate of direct arrival of downgoing focusing wavefield. Then the Green's functions are obtained from Eq. (2-14) and Eq. (2-15).

2-3 Marchenko scheme including free-surface multiples and inhomogeneous overburden

The above scheme only takes account into internal multiples and no free-surface is assumed in the actual medium. Considering this problem, [Singh et al., 2015, Singh et al., 2017] extend the Marchenko equations to get the Green's functions including primaries, internal multiples as well as free-surface multiples in terms of acoustic flux and acoustic pressure, respectively. The actual medium is then indicated in Figure 2-5. Continuing with Eq. (2-14) and Eq. (2-15), the equations in terms of acoustic pressure then become [Singh et al., 2017]

$$G^-(\mathbf{x}_i, \mathbf{x}'_r, t) = \int_{\partial\mathbb{D}_r} d\mathbf{x} \int_{-\infty}^{t} [R(\mathbf{x}_r, \mathbf{x}'_r, t-t') f_1^+(\mathbf{x}_r, \mathbf{x}_i, t') - rR(\mathbf{x}_r, \mathbf{x}'_r, t-t') f_1^-(\mathbf{x}_r, \mathbf{x}_i, t')] dt' - f_1^-(\mathbf{x}_r, \mathbf{x}_i, t), \tag{2-20}$$

$$G^+(\mathbf{x}_i, \mathbf{x}'_r, t) = -\int_{\partial\mathbb{D}_r} d\mathbf{x} \int_{-\infty}^{t} [R(\mathbf{x}_r, \mathbf{x}'_r, t-t') f_1^-(\mathbf{x}_r, \mathbf{x}_i, -t') - rR(\mathbf{x}_r, \mathbf{x}'_r, t-t') f_1^+(\mathbf{x}_r, \mathbf{x}_i, -t')] dt' + f_1^+(\mathbf{x}_r, \mathbf{x}_i, -t), \tag{2-21}$$

where r is the reflection coefficient of the free surface and $R(\mathbf{x}_r, \mathbf{x}'_r, t)$ includes free-surface multiples. By solving the above Marchenko equations, the retrieved Green's functions include accurate estimate of free-surface multiples.

Later in [Slob and Wapenaar, 2017, Ravasi, 2017], they proposed a redatuming scheme considering different source and receiver depth levels (Figure 2-6) for marine data. We redefine this state as state B. The relations for marine data in terms of acoustic pressure and vertical

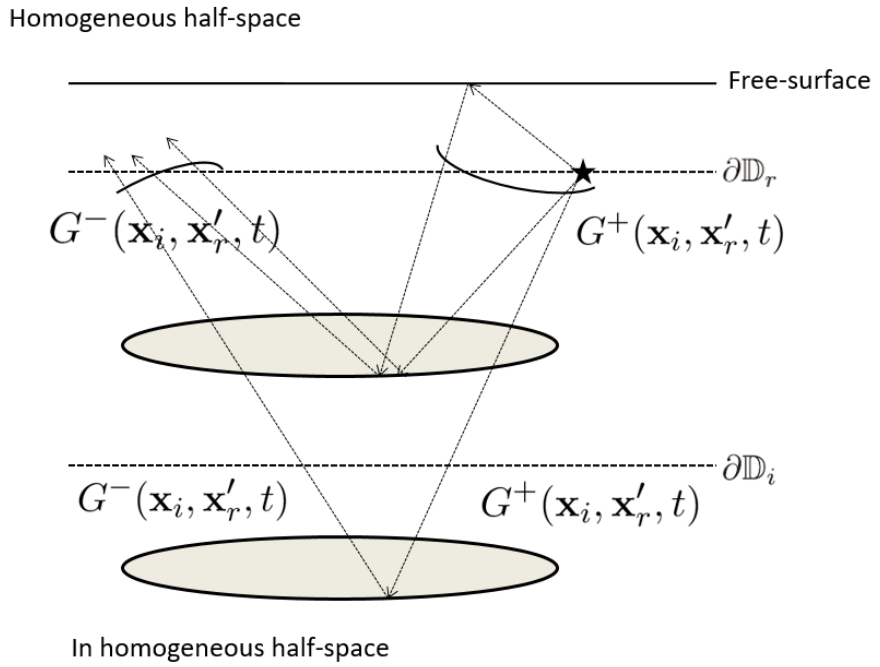

Figure 2-5: Downgoing and upgoing Green's functions in the actual medium including a free surface

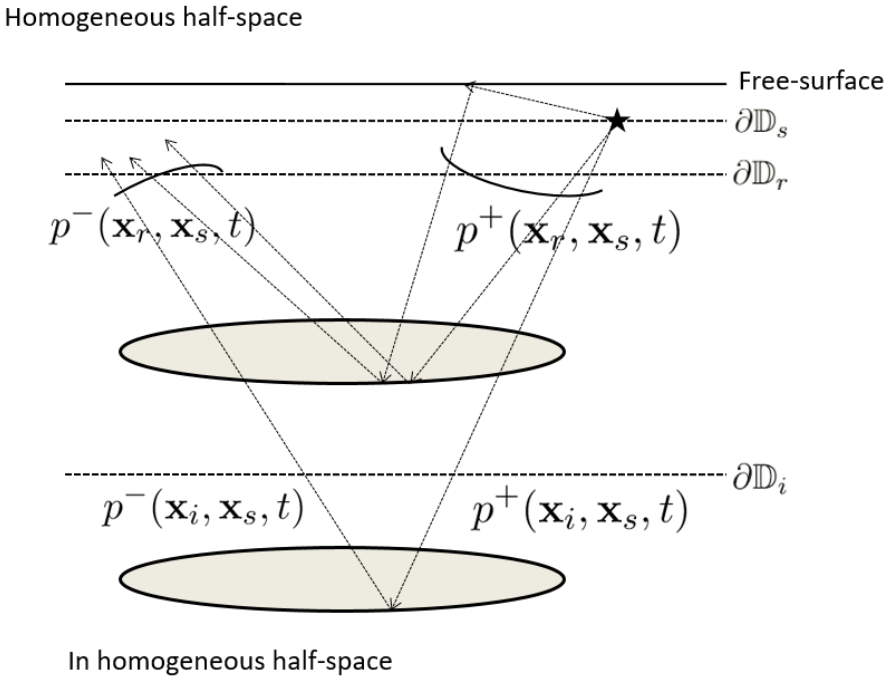

Figure 2-6: Downgoing and upgoing Green's functions in the actual medium including a free surface with different source and receiver depth levels

particle velocity are given by [Slob and Wapenaar, 2017]

$$p^-(\mathbf{x}_i,\mathbf{x}_s,t) = -2\int_{\partial\mathbb{D}_r}\int_{t'=-\infty}^{t}[f_1^+(\mathbf{x}_r,\mathbf{x}_i,t')v_z^-(\mathbf{x}_r,\mathbf{x}_s,t-t') + f_1^-(\mathbf{x}_r,\mathbf{x}_i,t')v_z^+(\mathbf{x}_r,\mathbf{x}_s,t-t')]dt'd\mathbf{x}_r, \tag{2-22}$$

$$p^+(\mathbf{x}_i,\mathbf{x}_s,t) = 2\int_{\partial\mathbb{D}_r}\int_{t'=-\infty}^{t}[f_1^+(\mathbf{x}_r,\mathbf{x}_i,-t')v_z^+(\mathbf{x}_r,\mathbf{x}_s,t-t') + f_1^-(\mathbf{x}_r,\mathbf{x}_i,-t')v_z^-(\mathbf{x}_r,\mathbf{x}_s,t-t')]dt'd\mathbf{x}_r, \tag{2-23}$$

where $p^\pm$ are one-way acoustic pressure fields, $v_z^\pm$ are one-way velocity fields and $f_1^\pm$ are pressure-related focusing functions. Eq. (2-22) and Eq. (2-23) can be used as a general scheme for up- and downgoing decomposed data at any depth level.

Chapter 3

Marchenko-type Equations With Two-Way Wavefields at the Receiver Level

As mentioned above, the reciprocity theorems for one-way wavefields can be used for the derivation of one-way Marchenko equations. The biggest issue is that it requires work to be done on the data before one can use the scheme. A new option then appears that we can use a different pattern of reciprocity theorems by leaving data at the receiver level unchanged but only normalizing data at the focusing level in order to utilize the focusing condition. This avoids that we have to make assumptions about the medium at the receiver level, which can be problematic e.g., for ocean bottom nodes or cables that are in contact with or even partially inside the seabed.

3-1 Normalization options at the focusing level

The reciprocity theorems for two-way wavefields are given as [T. de Hoop, 1995]

$$\begin{aligned}&\int_{\partial\mathbb{D}_r}[\hat{p}_A(\mathbf{x}_r)\hat{v}_{z,B}(\mathbf{x}_r)-\hat{p}_B(\mathbf{x}_r)\hat{v}_{z,A}(\mathbf{x}_r)]d\mathbf{x}_r\\&=\int_{\partial\mathbb{D}_i}[\hat{p}_A(\mathbf{x}_i)\hat{v}_{z,B}(\mathbf{x}_i)-\hat{p}_B(\mathbf{x}_i)\hat{v}_{z,A}(\mathbf{x}_i)]d\mathbf{x}_i,\end{aligned}\tag{3-1}$$

$$\begin{aligned}&\int_{\partial\mathbb{D}_r}[(\hat{p}_A(\mathbf{x}_r))^*\hat{v}_{z,B}(\mathbf{x}_r)+\hat{p}_B(\mathbf{x}_r)(\hat{v}_{z,A}(\mathbf{x}_r))^*]d\mathbf{x}_r\\&=\int_{\partial\mathbb{D}_i}[(\hat{p}_A(\mathbf{x}_i))^*\hat{v}_{z,B}(\mathbf{x}_i)+\hat{p}_B(\mathbf{x}_i)(\hat{v}_{z,A}(\mathbf{x}_i))^*]d\mathbf{x}_i,\end{aligned}\tag{3-2}$$

which become the basis of the following versions considering different normalization choices as shown in Figure 2-2 at the focusing level. For Eq. (3-1) and Eq. (3-2), we keep the left-hand side products unchanged and only look at the decomposition of the right-hand side

products at the focusing level. Using pressure-normalization, the relations between one-way and two-way wavefields at the focusing level are

$$\hat{p} = \hat{p}^+ + \hat{p}^-, \tag{3-3}$$

$$\hat{v}_z = -\frac{1}{j\omega\rho}\partial_z(\hat{p}^+ + \hat{p}^-). \tag{3-4}$$

According to Parceval's relation, the product in the right-hand side of Eq. (3-1) can be transformed into wavenumber-frequency domain as

$$\begin{aligned}&\int_{\partial\mathbb{D}_i}[\hat{p}_A(\mathbf{x}_i)\hat{v}_{z,B}(\mathbf{x}_i) - \hat{p}_B(\mathbf{x}_i)\hat{v}_{z,A}(\mathbf{x}_i)]d\mathbf{x}_i\\ &= \int_{\partial\mathbb{D}_i}[\tilde{p}_A(k_{x,i},k_{y,i},z_i)\tilde{v}_{z,B}(k_{x,i},k_{y,i},z_i) - \tilde{p}_B(k_{x,i},k_{y,i},z_i)\tilde{v}_{z,A}(k_x,k_y,z)]dk_{x,i}dk_{y,i},\end{aligned} \tag{3-5}$$

where $k_{x,i}$ and $k_{y,i}$ are horizontal wavenumbers at the focusing level.. We assume that ρ is almost constant at $\partial\mathbb{D}_i$ which yields

$$\tilde{p}(z_i) = \tilde{p}^+(z_i) + \tilde{p}^-(z_i), \tag{3-6}$$

$$\tilde{v}_z(z_i) \approx -\frac{1}{j\omega\rho(z_i)}\partial_z(\tilde{p}^+(z_i) + \tilde{p}^-(z_i)), \tag{3-7}$$

With further assumption that c is almost constant at $\partial\mathbb{D}_i$, the propagation of monochromatic one-way acoustic pressure can be expressed as [Wapenaar and Berkhout, 1989]

$$\tilde{p}^\pm(z_i) \approx \tilde{A}^\pm e^{\mp\Gamma(z_i)}, \tag{3-8}$$

where $\tilde{A}^\pm$ don't vary with z and

$$\Gamma = \begin{cases} j\sqrt{\frac{\omega^2}{c^2} - k_{x,i}^2 - k_{y,i}^2} & for \quad propagating \quad field \\ \sqrt{k_{x,i}^2 + k_{y,i}^2 - \frac{\omega^2}{c^2}} & for \quad evanescent \quad field \end{cases}, \tag{3-9}$$

see the Appendix in [Wapenaar and Berkhout, 1989]. With further assumption that c is smoothly varying with depth we have $\partial_z\tilde{p}^\pm \approx \mp\Gamma\tilde{p}^\pm$. We can then further express $\tilde{v}$ according to

$$\tilde{v}_z(z_i) \approx \frac{\Gamma}{j\omega\rho}(\tilde{p}^+(z_i) - \tilde{p}^-(z_i)). \tag{3-10}$$

Substituting Eq. (3-6) and Eq. (3-10) into the right-hand side of Eq. (3-5), we obtain

$$\begin{aligned}&\int_{\partial\mathbb{D}_i}(\tilde{p}_A\tilde{v}_{z,B} - \tilde{p}_B\tilde{v}_{z,A})dk_{x,i}dk_{y,i}\\ &= \int_{\partial\mathbb{D}_i}[(\tilde{p}_A^+ + \tilde{p}_A^-)\frac{\Gamma}{j\omega\rho}(\tilde{p}_B^+ - \tilde{p}_B^-) - (\tilde{p}_B^+ + \tilde{p}_B^-)\frac{\Gamma}{j\omega\rho}(\tilde{p}_A^+ - \tilde{p}_A^-)]dk_{x,i}dk_{y,i}.\end{aligned} \tag{3-11}$$

Then for the right-hand side of Eq. (3-2), we perform the same procedures above. Additionally, we give the complex conjugate version of Eq. (3-10) as

$$(\tilde{v}_z(z_i))^* \approx \begin{cases} \frac{\Gamma}{j\omega\rho}(\tilde{p}^+(z_i) - \tilde{p}^-(z_i))^* & for \quad propagating \quad field \\ -\frac{\Gamma}{j\omega\rho}(\tilde{p}^+(z_i) - \tilde{p}^-(z_i))^* & for \quad evanescent \quad field \end{cases}. \tag{3-12}$$

This is because for propagating waves $\frac{\Gamma}{j\omega\rho}$ is a real number so that we can keep it unchanged while for evanescent waves $\frac{\Gamma}{j\omega\rho}$ is an imaginary number of which the complex conjugate has a minus sign. The expression for the right-hand side of Eq. (3-2) then becomes

$$\begin{aligned}&\int_{\partial\mathbb{D}_i}[(\tilde{p}_A)^*\tilde{v}_{z,B}+\tilde{p}_B(\tilde{v}_{z,A})^*]dk_{x,i}dk_{y,i}\\&\approx\int_{\partial\mathbb{D}_i}[(\tilde{p}_A^+ + \tilde{p}_A^-)^*\frac{\Gamma}{j\omega\rho}(\tilde{p}_B^+ - \tilde{p}_B^-)+(\tilde{p}_B^+ + \tilde{p}_B^-)\frac{\Gamma}{j\omega\rho}(\tilde{p}_A^+ - \tilde{p}_A^-)^*]dk_{x,i}dk_{y,i},\end{aligned} \tag{3-13}$$

where we assume the evanescent waves are negligible at the focusing level. Based on Eq. (3-11), we can choose to apply the factor $\frac{\Gamma}{j\omega\rho}$ on different items according to the normalization methods we choose. Here we give the corresponding representations for one-way wavefields in terms of acoustic pressure, velocity and flux normalization as

$$\tilde{p}^{\pm} = \tilde{p}^{\pm}, \tag{3-14}$$

$$\tilde{v}_z^{\pm} = \pm\frac{\Gamma}{j\omega\rho}\tilde{p}^{\pm}, \tag{3-15}$$

$$\tilde{p}^{f,\pm} = (\frac{2\Gamma}{j\omega\rho})^{\frac{1}{2}}\tilde{p}^{\pm}, \tag{3-16}$$

where $\tilde{p}^{\pm}$ are pressure-normalized wavefields, $\tilde{v}^{\pm}$ are velocity-normalized wavefields and $\tilde{p}^{f,\pm}$ are flux-normalized wavefields. Under the assumptions explained above, if we apply the factor $\frac{\Gamma}{j\omega\rho}$ on state A, we can actually obtain the right-hand sides of Eq. (2-8) and Eq. (2-9). And for our scheme, we transform Eq. (3-11) and Eq. (3-13) to space-frequency domain and substituting them into Eq. (3-1) and Eq. (3-2) yielding

$$\begin{aligned}&\int_{\partial\mathbb{D}_r}[\hat{p}_A(\mathbf{x}_r)\hat{v}_{z,B}(\mathbf{x}_r)-\hat{p}_B(\mathbf{x}_r)\hat{v}_{z,A}(\mathbf{x}_r)]d\mathbf{x}_r\\&=-2\int_{\partial\mathbb{D}_i}[\hat{v}_{z,A}^+(\mathbf{x}_i)\hat{p}_B^-(\mathbf{x}_i)+\hat{v}_{z,A}^-(\mathbf{x}_i)\hat{p}_B^+(\mathbf{x}_i)]d\mathbf{x}_i,\end{aligned} \tag{3-17}$$

$$\begin{aligned}&\int_{\partial\mathbb{D}_r}[(\hat{p}_A(\mathbf{x}_r))^*\hat{v}_{z,B}(\mathbf{x}_r)+\hat{p}_B(\mathbf{x}_r)(\hat{v}_{z,A}(\mathbf{x}_r))^*]d\mathbf{x}_r\\&=2\int_{\partial\mathbb{D}_i}[(\hat{v}_{z,A}^+(\mathbf{x}_i))^*\hat{p}_B^+(\mathbf{x}_i)+(\hat{v}_{z,A}^-(\mathbf{x}_i))^*\hat{p}_B^-(\mathbf{x}_i)]d\mathbf{x}_i.\end{aligned} \tag{3-18}$$

Accordingly, if we want wavefields in state A to be pressure while wavefields in state B to be velocity, we obtain

$$\begin{aligned}&\int_{\partial\mathbb{D}_r}[\hat{p}_A(\mathbf{x}_r)\hat{v}_{z,B}(\mathbf{x}_r)-\hat{p}_B(\mathbf{x}_r)\hat{v}_{z,A}(\mathbf{x}_r)]d\mathbf{x}_r\\&=2\int_{\partial\mathbb{D}_i}[\hat{p}_A^+(\mathbf{x}_i)\hat{v}_{z,B}^-(\mathbf{x}_i)+\hat{p}_A^-(\mathbf{x}_i)\hat{v}_{z,B}^+(\mathbf{x}_i)]d\mathbf{x}_i,\end{aligned} \tag{3-19}$$

$$\begin{aligned}&\int_{\partial\mathbb{D}_r}[(\hat{p}_A(\mathbf{x}_r))^*\hat{v}_{z,B}(\mathbf{x}_r)+\hat{p}_B(\mathbf{x}_r)(\hat{v}_{z,A}(\mathbf{x}_r))^*]d\mathbf{x}_r\\&=2\int_{\partial\mathbb{D}_i}[(\hat{p}_A^+(\mathbf{x}_i))^*\hat{v}_{z,B}^+(\mathbf{x}_i)+(\hat{p}_A^-(\mathbf{x}_i))^*\hat{v}_{z,B}^-(\mathbf{x}_i)]d\mathbf{x}_i.\end{aligned} \tag{3-20}$$

And if we choose both wavefields in state A and state B to be flux-normalized fields, the representation theorems become

$$\begin{aligned}&\int_{\partial\mathbb{D}_r}[\hat{p}_A(\mathbf{x}_r)\hat{v}_{z,B}(\mathbf{x}_r)-\hat{p}_B(\mathbf{x}_r)\hat{v}_{z,A}(\mathbf{x}_r)]d\mathbf{x}_r\\&=-\int_{\partial\mathbb{D}_i}[\hat{p}_A^{f,+}(\mathbf{x}_i)\hat{p}_B^{f,-}(\mathbf{x}_i)-\hat{p}_A^{f,-}(\mathbf{x}_i)\hat{p}_B^{f,+}(\mathbf{x}_i)]d\mathbf{x}_i,\end{aligned}\tag{3-21}$$

$$\begin{aligned}&\int_{\partial\mathbb{D}_r}[(\hat{p}_A(\mathbf{x}_r))^*\hat{v}_{z,B}(\mathbf{x}_r)+\hat{p}_B(\mathbf{x}_r)(\hat{v}_{z,A}(\mathbf{x}_r))^*]d\mathbf{x}_r\\&=\int_{\partial\mathbb{D}_i}[(\hat{p}_A^{f,+}(\mathbf{x}_i))^*\hat{p}_B^{f,+}(\mathbf{x}_i)-(\hat{p}_A^{f,-}(\mathbf{x}_i))^*\hat{p}_B^{f,-}(\mathbf{x}_i)]d\mathbf{x}_i.\end{aligned}\tag{3-22}$$

Now the question is that why would we want one of those options. The answer is that it depends on which wavefield we want to focus. That choice has a consequence on the retrieved pressure and velocity focusing functions. In the coming sections we will discuss this.

3-2 Revised Marchenko-type equations with flux-normalized one-way wavefields at the focusing level

In this section, we choose flux-normalization of the wavefields in both state A and B and use Eq. (3-21) and Eq. (3-22). At the receiver level, we define the two-way wavefields $\hat{p}_A$ and $\hat{v}_{z,A}$ in state A as focusing functions $\hat{f}^f$ and $\hat{g}^f$ while $\hat{p}_B$ and $\hat{v}_{z,B}$ are replaced with $\hat{p}$ and $\hat{v}_z$ for the sake of simplicity. At the focusing level, we replace $\hat{p}_B^{f,\pm}$ with $\hat{p}^{f,\pm}$ and choose to focus the flux-normalized wavefields as

$$\hat{p}_A^{f,+}(\mathbf{x}_i',\mathbf{x}_i)|_{(x_{z,i}'=x_{z,i})}=\delta(\mathbf{x}_{H,i}'-\mathbf{x}_{H,i}),\tag{3-23}$$

$$\hat{p}_A^{f,-}(\mathbf{x}_i',\mathbf{x}_i)|_{(x_{z,i}'=x_{z,i})}=0.\tag{3-24}$$

Notice that the choice of focusing condition in this scheme determines the space-time behavior of the retrieved focusing functions $\hat{f}$ and $\hat{g}$. We use the superscript ^{f} to represent that the focusing functions are retrieved in such a way that the focusing condition is defined for flux-normalized one-way wavefields. The relations between focusing functions and $\hat{p}_A^{f,\pm}$ are given as

$$\hat{f}^f(\mathbf{x}_i)=(\frac{\omega\rho}{2})^{\frac{1}{2}}\hat{\mathcal{H}}_1^{-\frac{1}{2}}(\hat{p}_A^{f,+}(\mathbf{x}_i)+\hat{p}_A^{f,-}(\mathbf{x}_i)),\tag{3-25}$$

$$\hat{g}^f(\mathbf{x}_i)=(2\omega\rho)^{-\frac{1}{2}}\hat{\mathcal{H}}_1^{\frac{1}{2}}(\hat{p}_A^{f,+}(\mathbf{x}_i)-\hat{p}_A^{f,-}(\mathbf{x}_i)),\tag{3-26}$$

where $\hat{\mathcal{H}}_1$ is defined as the square-root operator according to [Wapenaar et al., 2014b]

$$\partial_z\hat{p}^{\pm}=\mp j\hat{\mathcal{H}}_1\hat{p}^{\pm}.\tag{3-27}$$

This leads to the following relations

$$\hat{p}^{f,-}(\mathbf{x}_i,\mathbf{x}_s)=-\int_{\partial\mathbb{D}_r}[\hat{f}^f(\mathbf{x}_r,\mathbf{x}_i)\hat{v}_z(\mathbf{x}_r,\mathbf{x}_s)-\hat{g}^f(\mathbf{x}_r,\mathbf{x}_i)\hat{p}(\mathbf{x}_r,\mathbf{x}_s)]d\mathbf{x}_r,\tag{3-28}$$

$$\hat{p}^{f,+}(\mathbf{x}_i,\mathbf{x}_s)=\int_{\partial\mathbb{D}_r}[(\hat{f}^f(\mathbf{x}_r,\mathbf{x}_i))^*\hat{v}_z(\mathbf{x}_r,\mathbf{x}_s)+(\hat{g}^f(\mathbf{x}_r,\mathbf{x}_i))^*\hat{p}(\mathbf{x}_r,\mathbf{x}_s)]d\mathbf{x}_r. \tag{3-29}$$

In time domain we have equations given by

$$\begin{aligned}&p^{f,-}(\mathbf{x}_i,\mathbf{x}_s,t)\\&=-\int_{\partial\mathbb{D}_r}\int_{-\infty}^{t}[f^f(\mathbf{x}_r,\mathbf{x}_i,t')v_z(\mathbf{x}_r,\mathbf{x}_s,t-t')-g^f(\mathbf{x}_r,\mathbf{x}_i,t')p(\mathbf{x}_r,\mathbf{x}_s,t-t')]d\mathbf{x}_r dt',\end{aligned} \tag{3-30}$$

$$\begin{aligned}&p^{f,+}(\mathbf{x}_i,\mathbf{x}_s,t)\\&=\int_{\partial\mathbb{D}_r}\int_{-\infty}^{t}[f^f(\mathbf{x}_r,\mathbf{x}_i,-t')v_z(\mathbf{x}_r,\mathbf{x}_s,t-t')+g^f(\mathbf{x}_r,\mathbf{x}_i,-t')p(\mathbf{x}_r,\mathbf{x}_s,t-t')]d\mathbf{x}_r dt'.\end{aligned} \tag{3-31}$$

For $t<t_d(\mathbf{x}_i,\mathbf{x}_s)$, the left-hand sides are zero in Eq. (3-30) and Eq. (3-31) since $t_d(\mathbf{x}_i,\mathbf{x}_s)$ is the time when the direct wavefield arrives at the focusing point $\mathbf{x}_i$. In the right-hand sides of Eq. (3-30), the focusing wavefields start to exist at $t=-t_d(\mathbf{x}_i,\mathbf{x}_r)$ and vanish for $t>t_d(\mathbf{x}_i,\mathbf{x}_r)$. In the right-hand side of Eq. (3-31), when $t=t_d(\mathbf{x}_i,\mathbf{x}_r)$ both $f^f(-t_d)$ and $g^f(-t_d)$ are non-zero. So, we need to exclude time instant $t_d(\mathbf{x}_i,\mathbf{x}_r)$. For $t<t_d(\mathbf{x}_i,\mathbf{x}_s)$, Eq. (3-30) and Eq. (3-31) are restricted to

$$0=\int_{\partial\mathbb{D}_r}\int_{-t_d}^{t}[f^f(\mathbf{x}_r,\mathbf{x}_i,t')v_z(\mathbf{x}_r,\mathbf{x}_s,t-t')-g^f(\mathbf{x}_r,\mathbf{x}_i,t')p(\mathbf{x}_r,\mathbf{x}_s,t-t')]d\mathbf{x}_r dt', \tag{3-32}$$

$$0=\int_{\partial\mathbb{D}_r}\int_{-t_d}^{t}[f^f(\mathbf{x}_r,\mathbf{x}_i,-t')v_z(\mathbf{x}_r,\mathbf{x}_s,t-t')+g^f(\mathbf{x}_r,\mathbf{x}_i,-t')p(\mathbf{x}_r,\mathbf{x}_s,t-t')]d\mathbf{x}_r dt', \tag{3-33}$$

from which we can solve for $f^f(\mathbf{x}_r,\mathbf{x}_i,t)$ and $g^f(\mathbf{x}_r,\mathbf{x}_i,t)$ in the time interval $-t_d(\mathbf{x}_i,\mathbf{x}_r)\le t<t_d(\mathbf{x}_i,\mathbf{x}_r)$ with the need of estimate of direct arrival part of acoustic pressure and vertical particle velocity related focusing functions $f_d^{f,+}(\mathbf{x}_r,\mathbf{x}_i,t_d)$ and $g_d^{f,+}(\mathbf{x}_r,\mathbf{x}_i,t_d)$ in the actual fields since we exclude the time instance $t_d(\mathbf{x}_i,\mathbf{x}_r)$. To obtain the solution, we assume that $f^f(\mathbf{x}_r,\mathbf{x}_i,t)$ and $g^f(\mathbf{x}_r,\mathbf{x}_i,t)$ can be written as a direct wave plus a scattering coda

$$f^f(\mathbf{x}_r,\mathbf{x}_i,t)=f_d^{f,+}(\mathbf{x}_r,\mathbf{x}_i,t)+f_m^f(\mathbf{x}_r,\mathbf{x}_i,t), \tag{3-34}$$

$$g^f(\mathbf{x}_r,\mathbf{x}_i,t)=g_d^{f,+}(\mathbf{x}_r,\mathbf{x}_i,t)+g_m^f(\mathbf{x}_r,\mathbf{x}_i,t), \tag{3-35}$$

where $f_d^{f,+}(\mathbf{x}_r,\mathbf{x}_i,t)$ and $g_d^{f,+}(\mathbf{x}_r,\mathbf{x}_i,t)$ denote the direct arrival parts of both focusing wavefields. Instead of estimating $f_d^{f,+}(\mathbf{x}_r,\mathbf{x}_i,t)$ and $g_d^{f,+}(\mathbf{x}_r,\mathbf{x}_i,t)$, we can just find the evaluation of $p_{A,d}^{f,+}$ which is the direct arrival of the downgoing flux-normalized focusing function. To explain this, we first write the separated multiplication products of direct focusing wavefields with data in wavenumber-frequency and derive the following relations as

$$\begin{aligned}&\int_{\partial\mathbb{D}_r}(\tilde{g}_d^{f,+}\tilde{p}-\tilde{f}_d^{f,+}\tilde{v}_z)dk_{k,r}dk_{y,r}\\&\approx\int_{\partial\mathbb{D}_r}[(\frac{\Gamma}{j\omega\rho})^{\frac{1}{2}}\tilde{p}_{A,d}^{f,+}(\tilde{p}^+ +\tilde{p}^-)-(\frac{\Gamma}{j\omega\rho})^{-\frac{1}{2}}\tilde{p}_{A,d}^{f,+}(\tilde{v}_z^+ +\tilde{v}_z^-)]dk_{k,r}dk_{y,r}\\&\approx\int_{\partial\mathbb{D}_r}[\tilde{p}_{A,d}^{f,+}((\frac{\Gamma}{j\omega\rho})^{\frac{1}{2}}(\tilde{p}^+ +\tilde{p}^-)-(\frac{\Gamma}{j\omega\rho})^{-\frac{1}{2}}(\tilde{v}_z^+ +\tilde{v}_z^-))]dk_{k,r}dk_{y,r}\\&=\int_{\partial\mathbb{D}_r}2(\tilde{p}_{A,d}^{f,+}\tilde{p}^{f,-})dk_{k,r}dk_{y,r}.\end{aligned} \tag{3-36}$$

According to [Wapenaar et al., 2014a], we have the relations

$$p^{f,+}_{A,d}(\mathbf{x}_r,\mathbf{x}_i,t)=T^{f,inv}_d(\mathbf{x}_i,\mathbf{x}_r,t), \tag{3-37}$$

where $T^{f,inv}_d$ is the inverse of the transmission response from $\mathbf{x}_r$ to $\mathbf{x}_i$ which can be approximately evaluated by the estimate of time reversal of downgoing flux-normalized Green's function $G^{f,+}_d(\mathbf{x}_r,\mathbf{x}_i,-t)$. We can see that with the above assumptions, we can move the operator $(\frac{\Gamma}{j\omega\rho})^{\frac{1}{2}}$ and $(\frac{\Gamma}{j\omega\rho})^{-\frac{1}{2}}$ around to apply them on pressure and vertical particle velocity, respectively. Then we only need the estimate of flux-normalized downgoing wavefield which is $G^{f,+}_d$ as well as $p^{f,-}$. Then we can revise Eq. (3-32) and Eq. (3-33) to

$$\begin{aligned}&\int_{\partial\mathbb{D}_r}2(G^{f,+}_d(\mathbf{x}_r,\mathbf{x}_i,-t_d)p^{f,-}(\mathbf{x}_r,\mathbf{x}_s,t+t_d)d\mathbf{x}_r\\&=\int_{\partial\mathbb{D}_r}\int_{-t_d}^{t}[f^f_m(\mathbf{x}_r,\mathbf{x}_i,t')v_z(\mathbf{x}_r,\mathbf{x}_s,t-t')-g^f_m(\mathbf{x}_r,\mathbf{x}_i,t')p(\mathbf{x}_r,\mathbf{x}_s,t-t')]d\mathbf{x}_r dt',\end{aligned} \tag{3-38}$$

$$0=\int_{\partial\mathbb{D}_r}\int_{t'=-t}^{t_d}[f^f_m(\mathbf{x}_r,\mathbf{x}_i,t')v_z(\mathbf{x}_r,\mathbf{x}_s,t+t')+g^f_m(\mathbf{x}_r,\mathbf{x}_i,t')p(\mathbf{x}_r,\mathbf{x}_s,t+t')]d\mathbf{x}_r dt'. \tag{3-39}$$

For the two-way Marchenko-type equations, we don't need any assumption at the data level. However, the computation procedure becomes unstable due to the large magnitude difference between acoustic pressure and vertical particle velocity. The impedance difference is roughly 10^6 at the data level and hence we take $v_{z,new}=10^6 v_z$ and the retrieved pressure-related focusing function $f^f_{m,new}$ is then equal to $\frac{f^f_m}{10^6}$. This easily solves the amplitude unbalance problem.

Now we come back to the implementation of Eq. (3-38) and Eq. (3-39). The estimate of the direct arrival can be done by performing numerical modelling on a macro model with the source at the focusing point $\mathbf{x}_i$. For measured data, the right side of the time window should be adjusted to $t_d+\epsilon$ and the left-hand side of the time window should be adjusted to $-t_d-\epsilon$ to account for the finite bandwidth.

3-3 Revised Marchenko-typed equations with velocity-normalized one-way wavefields at the focusing level

For velocity-normalized data in state B at the focusing level, the downgoing and upgoing waves are normalized such that their sum is equal to the vertical particle velocity v_z and we use Eq. (3-19) and Eq. (3-20). At the receiver level, we still use the same replacements as above but change the superscript from ^{f} to ^{p} for focusing functions while at the focusing level, we replace $\hat{v}^{\pm}_{z,B}$ with $\hat{v}^{\pm}_z$ and choose to focus the pressure-normalized wavefields as

$$\hat{p}^{+}_A(\mathbf{x}'_i,\mathbf{x}_i)|_{(x'_{z,i}=x_{z,i})}=\frac{1}{2}\delta(\mathbf{x}'_{H,i}-\mathbf{x}_{H,i}), \tag{3-40}$$

$$\hat{p}^{-}_A(\mathbf{x}'_i,\mathbf{x}_i)|_{(x'_{z,i}=x_{z,i})}=0. \tag{3-41}$$

With this choice, we give the relations between the focusing functions and $\hat{p}^{\pm}_A$ as

$$\hat{f}^p(\mathbf{x}_i)=\hat{p}^{+}_A(\mathbf{x}_i)+\hat{p}^{-}_A(\mathbf{x}_i), \tag{3-42}$$

$$\hat{g}^p(\mathbf{x}_i) = \frac{\hat{\mathcal{H}}_1}{\omega\rho}(\hat{p}_A^+(\mathbf{x}_i) - \hat{p}_A^-(\mathbf{x}_i)). \tag{3-43}$$

It is worth mentioning that $\hat{f}^p$ and $\hat{g}^p$ are still pressure and velocity focusing functions but under the focusing condition for pressure-normalized wavefields. Substituting them into Eq. (3-19) and Eq. (3-20), we obtain

$$\hat{v}_z^-(\mathbf{x}_i, \mathbf{x}_s) = \int_{\partial\mathbb{D}_r} [\hat{f}^p(\mathbf{x}_r, \mathbf{x}_i)\hat{v}_z(\mathbf{x}_r, \mathbf{x}_s) - \hat{g}^p(\mathbf{x}_r, \mathbf{x}_i)\hat{p}(\mathbf{x}_r, \mathbf{x}_s)]d\mathbf{x}_r, \tag{3-44}$$

$$\hat{v}_z^+(\mathbf{x}_i, \mathbf{x}_s) = \int_{\partial\mathbb{D}_r} [(\hat{f}^p(\mathbf{x}_r, \mathbf{x}_i))^*\hat{v}_z(\mathbf{x}_r, \mathbf{x}_s) + (\hat{g}^p(\mathbf{x}_r, \mathbf{x}_i))^*\hat{p}(\mathbf{x}_r, \mathbf{x}_s)]d\mathbf{x}_r. \tag{3-45}$$

We transform them to space-time domain and apply the same time window as above on Eq. (3-44) and Eq. (3-45). This yields

$$0 = \int_{\partial\mathbb{D}_r}\int_{-t_d}^{t} [f^p(\mathbf{x}_r, \mathbf{x}_i, t')v_z(\mathbf{x}_r, \mathbf{x}_s, t-t') - g^p(\mathbf{x}_r, \mathbf{x}_i, t')p(\mathbf{x}_r, \mathbf{x}_s, t-t')]d\mathbf{x}_r dt', \tag{3-46}$$

$$0 = \int_{\partial\mathbb{D}_r}\int_{-t_d}^{t} [f^p(\mathbf{x}_r, \mathbf{x}_i, -t')v_z(\mathbf{x}_r, \mathbf{x}_s, t-t') + g^p(\mathbf{x}_r, \mathbf{x}_i, -t')p(\mathbf{x}_r, \mathbf{x}_s, t-t')]d\mathbf{x}_r dt', \tag{3-47}$$

This time we choose to use the approximate estimate of $f_d^{p,+}(\mathbf{x}_r, \mathbf{x}_i, t)$ which is the time reversal of pressure-normalized downgoing Green's function $G_d^{p,+}(\mathbf{x}_r, \mathbf{x}_i, -t)$ and then we have

$$\begin{aligned}&\int_{\partial\mathbb{D}_r} 2(G_d^{p,+}(\mathbf{x}_r, \mathbf{x}_i, -t_d)v_z^-(\mathbf{x}_r, \mathbf{x}_s, t+t_d)d\mathbf{x}_r \\ &= -\int_{\partial\mathbb{D}_r}\int_{-t_d}^{t} [f_m^p(\mathbf{x}_r, \mathbf{x}_i, t')v_z(\mathbf{x}_r, \mathbf{x}_s, t-t') - g_m^p(\mathbf{x}_r, \mathbf{x}_i, t')p(\mathbf{x}_r, \mathbf{x}_s, t-t')]d\mathbf{x}_r dt',\end{aligned} \tag{3-48}$$

$$0 = \int_{\partial\mathbb{D}_r}\int_{t'=-t}^{t_d} [f_m^p(\mathbf{x}_r, \mathbf{x}_i, t')v_z(\mathbf{x}_r, \mathbf{x}_s, t+t') + g_m^p(\mathbf{x}_r, \mathbf{x}_i, t')p(\mathbf{x}_r, \mathbf{x}_s, t+t')]d\mathbf{x}_r dt'. \tag{3-49}$$

Then Eq. (3-48) and Eq. (3-49) become the equations we solve to obtain the pressure and velocity related focusing functions f^p and g^p with the focusing condition chosen as to focus the pressure field.

3-4 Revised Marchenko-type equations with pressure-normalized one-way wavefields at the focusing level

For pressure-normalization method, the downgoing and upgoing waves are normalized such that their sum is equal to the pressure p in state B and we use Eq. (3-17) and Eq. (3-18). It can be derived in the same pattern as above. In this case, we replace $\hat{p}_B^{\pm}$ with $\hat{p}^{\pm}$ and change the superscript for focusing functions to ^{v} which means that we focus the velocity field according to

$$\hat{v}_{z,A}^+(\mathbf{x}_i', \mathbf{x}_i)|_{(x_{z,i}'=x_{z,i})} = \frac{1}{2}\delta(\mathbf{x}_{H,i}' - \mathbf{x}_{H,i}), \tag{3-50}$$

$$\hat{v}_{z,A}^-(\mathbf{x}_i', \mathbf{x}_i)|_{(x_{z,i}'=x_{z,i})} = 0, \tag{3-51}$$

with again the relations as

$$\hat{f}^v(\mathbf{x}_i) = \frac{\omega\rho}{\hat{\mathcal{H}}_1}(\hat{v}^+_{z,A}(\mathbf{x}_i) - \hat{v}^-_{z,A}(\mathbf{x}_i)), \tag{3-52}$$

$$\hat{g}^v(\mathbf{x}_i) = \hat{v}^+_{z,A}(\mathbf{x}_i) + \hat{v}^-_{z,A}(\mathbf{x}_i). \tag{3-53}$$

And here we have pressure and velocity focusing functions obtained from focusing the velocity field. Performing the same substitutions as those in the previous sections, we obtain

$$\hat{p}^-(\mathbf{x}_i, \mathbf{x}_s) = -\int_{\partial\mathbb{D}_r} [\hat{f}^v(\mathbf{x}_r, \mathbf{x}_i)\hat{v}_z(\mathbf{x}_r, \mathbf{x}_s) - \hat{g}^v(\mathbf{x}_r, \mathbf{x}_i)\hat{p}(\mathbf{x}_r, \mathbf{x}_s)]d\mathbf{x}_r, \tag{3-54}$$

$$\hat{p}^+(\mathbf{x}_i, \mathbf{x}_s) = \int_{\partial\mathbb{D}_r} [(\hat{f}^v(\mathbf{x}_r, \mathbf{x}_i))^*\hat{v}_z(\mathbf{x}_r, \mathbf{x}_s) + (\hat{g}^v(\mathbf{x}_r, \mathbf{x}_i))^*\hat{p}(\mathbf{x}_r, \mathbf{x}_s)]d\mathbf{x}_r, \tag{3-55}$$

Then we write the evaluated version of Eq. (3-54) and Eq. (3-55) in time domain with the same time window as

$$0 = \int_{\partial\mathbb{D}_r}\int_{-t_d}^{t} [f^v(\mathbf{x}_r, \mathbf{x}_i, t')v_z(\mathbf{x}_r, \mathbf{x}_s, t-t') - g^v(\mathbf{x}_r, \mathbf{x}_i, t')p(\mathbf{x}_r, \mathbf{x}_s, t-t')]d\mathbf{x}_r dt', \tag{3-56}$$

$$0 = \int_{\partial\mathbb{D}_r}\int_{-t_d}^{t} [f^v(\mathbf{x}_r, \mathbf{x}_i, -t')v_z(\mathbf{x}_r, \mathbf{x}_s, t-t') + g^v(\mathbf{x}_r, \mathbf{x}_i, -t')p(\mathbf{x}_r, \mathbf{x}_s, t-t')]d\mathbf{x}_r dt', \tag{3-57}$$

This time we choose to use the estimate of $f_d^{v,+}(\mathbf{x}_r, \mathbf{x}_i, t)$ which is the time reversal of velocity-normalized downgoing Green's function $G_d^{v,+}(\mathbf{x}_r, \mathbf{x}_i, -t)$ and then we have

$$\begin{aligned}&\int_{\partial\mathbb{D}_r} 2(G_d^{v,+}(\mathbf{x}_r, \mathbf{x}_i, -t_d)p^-(\mathbf{x}_r, \mathbf{x}_s, t+t_d)d\mathbf{x}_r \\ &= \int_{\partial\mathbb{D}_r}\int_{-t_d}^{t} [f_m^v(\mathbf{x}_r, \mathbf{x}_i, t')v_z(\mathbf{x}_r, \mathbf{x}_s, t-t') - g_m^v(\mathbf{x}_r, \mathbf{x}_i, t')p(\mathbf{x}_r, \mathbf{x}_s, t-t')]d\mathbf{x}_r dt',\end{aligned} \tag{3-58}$$

$$0 = \int_{\partial\mathbb{D}_r}\int_{t'=-t}^{t_d} [f_m^v(\mathbf{x}_r, \mathbf{x}_i, t')v_z(\mathbf{x}_r, \mathbf{x}_s, t+t') + g_m^v(\mathbf{x}_r, \mathbf{x}_i, t')p(\mathbf{x}_r, \mathbf{x}_s, t+t')]d\mathbf{x}_r dt'. \tag{3-59}$$

Then Eq. (3-58) and Eq. (3-59) become the equations we solve to obtain the pressure and velocity relate focusing functions f^v and g^v with the focusing condition chosen as to focus the velocity field.

To summarize, the scheme can be indicated as Figure 3-1.

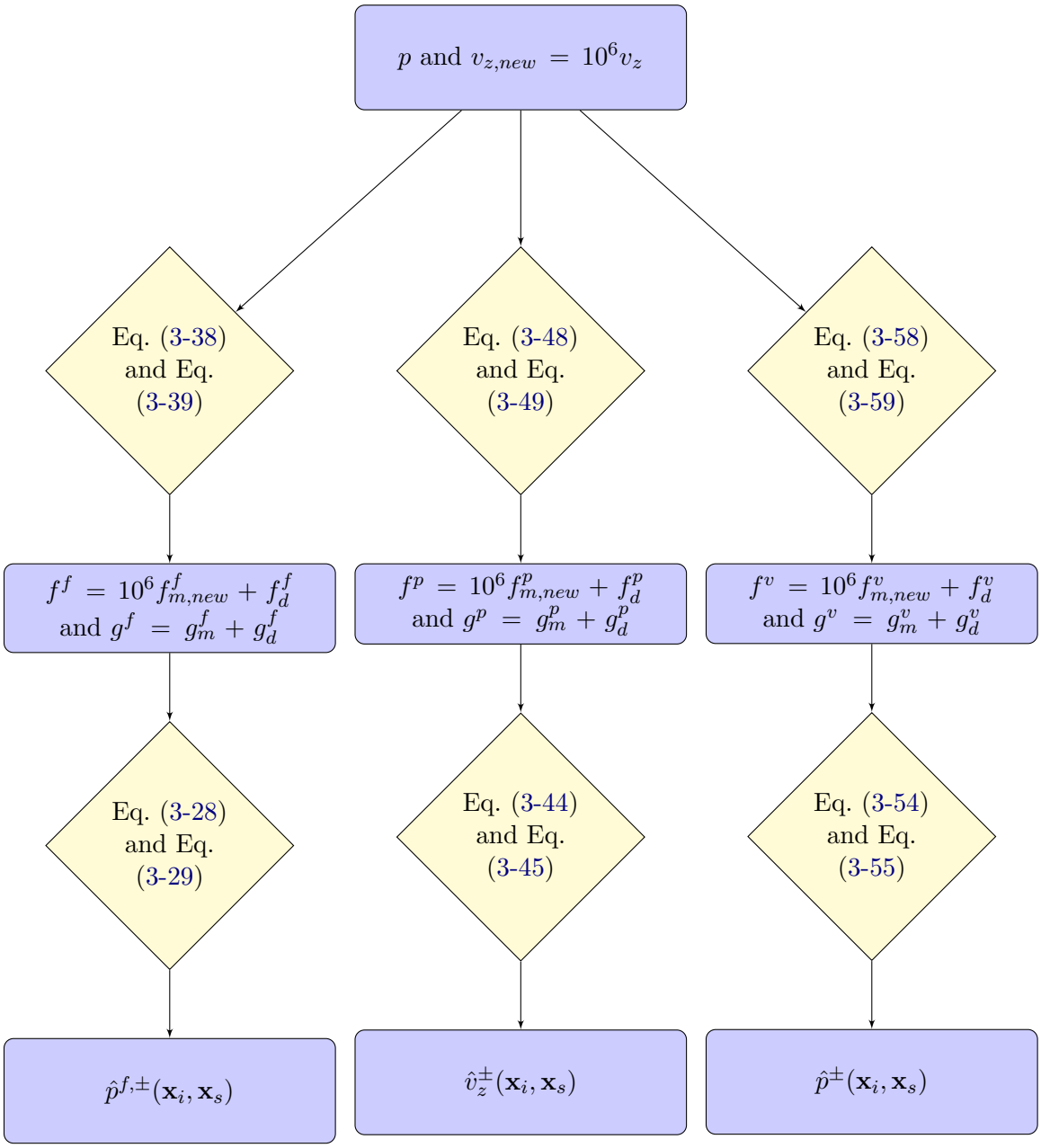

Figure 3-1: Flow chart for numerical solution procedure

Chapter 4

Numerical Examples

4-1 LSQR solving scheme

LSQR is an iterative method for solving the system of linear equation $A * x = b$ to find x if A is consistent. One of the conditions for A to be consistent is $rank(A) = rank(A|b)$ and another is that all solutions x of $A^T x = 0$ are orthogonal to b. If A is invertible, then the linear equation has the unique solution. The criterion of a stable solution is to enable $min||Ax-b||_2$ to be smaller than a predefined limit, for example, 10^{-3}. A common use of this method in Matlab is to construct the matrix A and right-hand column b as inputs. Then the solution of the function is x satisfying the criterion. Alternatively, one can also specify a function handle, such that $afun(x,'notransp')$ returns $y_1 = A * x$ and $afun(x,'transp')$ returns $y_2 = A^T * x$. Then the inputs become y_1 and y_2 with the same solution of x. The implementation details of both choices will be discussed in the following context of this subsection. We use the following representations for simplicity.
We take the implementation of coupled equations Eq. (3-38) and Eq. (3-39) in 1D situation as an example. The implementable 1D versions of Eq. (3-38) and Eq. (3-39) are given as

$$\begin{aligned}&\int_{-t_d}^{t}[v_{z,new}(z_r,z_s,t-t')f^f_{m,new}(z_r,z_i,t') - p(z_r,z_s,t-t')g^f_m(z_r,z_i,t')]dt' = \\ &2(G^{f,+}_d(z_r,z_i,t_d))^{-1}p^{f,-}(z_r,z_s,t+t_d),\end{aligned} \tag{4-1}$$

$$\int_{-t}^{t_d}[v_{z,new}(z_r,z_s,t+t')f^f_{m,new}(z_r,z_i,t') + p(z_r,z_s,t+t')g^f_m(z_r,z_i,t')]dt' = 0, \tag{4-2}$$

where $v_{z,new} = 10^6 v_z$ and $f^f_{m,new} = \frac{f^f_m}{10^6}$. We can further discretize the one-way arrival time using a sampling time $\Delta t \to 0$ and assume $t_d = n\Delta t$ and $t = k\Delta t$. The time range for t is limited according to $-n \le k \le n-1$ corresponding to $-t_d \le t < t_d$. Additionally, we define $t_{rs} = j\Delta t$ which represents the direct arrival time from source to receiver to account for the depth difference between them. Then the discrete equations for each constant value of n i.e.

each focusing depth can be written as

$$\begin{aligned}&\sum_{l=-n}^{k} v_{z,new}(j+k-l) f^{f}_{m,new}(n,l) - \sum_{l=-n}^{k} p(j+k-l) g^{f}_{m}(n,l)\\ &-\frac{1}{2}[v_{z,new}(j+k-k) f^{f}_{m,new}(n,k) - p(j+k-k) g^{f}_{m}(n,k)]\\ &= 2(G^{f,+}_{d}(n))^{-1} p^{f,-}(j+k+n),\end{aligned} \tag{4-3}$$

$$\begin{aligned}&\sum_{l=-k}^{n} v_{z,new}(j+k+l) f^{f}_{m,new}(n,l) + \sum_{l=-k}^{n} p(j+k+l) g^{f}_{m}(n,l)\\ &-\frac{1}{2}[v_{z,new}(j+k+n) f^{f}_{m,new}(n,n) + p(j+k+n) g^{f}_{m}(n,n)] = 0.\end{aligned} \tag{4-4}$$

In Eq. (4-3), the codas of focusing functions are 0 at $-t_d$ and the direct downgoing parts of the focusing functions are moved to the right-hand side which only exist at $-t_d$. And for Eq. (4-4), both direct arrivals and codas of the focusing functions are 0 at t_d so the right-hand side is 0. Then matrix form Eq. (4-3) and Eq. (4-4) can be written as

$$\begin{bmatrix} \frac{1}{2}v_{z,new}(j) & 0 & . & . & 0 \\ v_{z,new}(j+1) & \frac{1}{2}v_{z,new}(j) & 0 & . & 0 \\ . & . & . & 0 & 0 \\ . & . & . & . & 0 \\ v_{z,new}(j+2n-1) & . & . & v_{z,new}(j+1) & \frac{1}{2}v_{z,new}(j) \end{bmatrix} \times \begin{bmatrix} f^{f}_{m,new}(n,-n) \\ . \\ . \\ f^{f}_{m,new}(n,n-2) \\ f^{f}_{m,new}(n,n-1) \end{bmatrix}$$

$$- \begin{bmatrix} \frac{1}{2}p(j) & 0 & . & . & 0 \\ p(j+1) & \frac{1}{2}p(j) & 0 & . & 0 \\ . & . & . & 0 & 0 \\ . & . & . & . & 0 \\ p(j+2n-1) & . & . & p(j+1) & \frac{1}{2}p(j) \end{bmatrix} \times \begin{bmatrix} g^{f}_{m}(n,-n) \\ . \\ . \\ g^{f}_{m}(n,n-2) \\ g^{f}_{m}(n,n-1) \end{bmatrix}$$

$$= \begin{bmatrix} 2(G^{f,+}_{d}(n))^{-1} p^{f,-}(j) \\ . \\ . \\ 2(G^{f,+}_{d}(n))^{-1} p^{f,-}(j+2n-2) \\ 2(G^{f,+}_{d}(n))^{-1} p^{f,-}(j+2n-1) \end{bmatrix}, \tag{4-5}$$

$$\begin{bmatrix} 0 & 0 & . & 0 & \frac{1}{2}v_{z,new}(j) \\ 0 & . & 0 & v_{z,new}(j) & \frac{1}{2}v_{z,new}(j+1) \\ 0 & 0 & . & . & . \\ 0 & . & . & . & . \\ v_{z,new}(j) & v_{z,new}(j+1) & . & . & \frac{1}{2}v_{z,new}(j+2*n-1) \end{bmatrix} \times \begin{bmatrix} f^f_{m,new}(n,-n+1) \\ . \\ . \\ f^f_{m,new}(n,n-2) \\ f^f_{m,new}(n,n) \end{bmatrix}$$

$$+ \begin{bmatrix} 0 & 0 & . & 0 & \frac{1}{2}p(j) \\ 0 & . & 0 & p(j) & \frac{1}{2}p(j+1) \\ 0 & 0 & . & . & . \\ 0 & . & . & . & . \\ p(j) & p(j+1) & . & . & \frac{1}{2}p(j+2n-1) \end{bmatrix} \times \begin{bmatrix} g^f_m(n,-n+1) \\ . \\ . \\ g^f_m(n,n-2) \\ g^f_m(n,n) \end{bmatrix}$$

$$= \begin{bmatrix} 0 \\ . \\ . \\ 0 \\ 0 \end{bmatrix}. \tag{4-6}$$

This is a matrix system containing $2n$ equations t be solved. Here we need to emphasis that since the codas of both focusing functions are 0 at t_d and $-t_d$ which are $f^f_{m,new}(n,\pm n)$ and $g^f_m(n,\pm n)$, Eq. (4-5) and Eq. (4-6) actually contains the same focusing functions excluding time instances $-t_d$ and t_d, respectively. Then the number of equations to be solved becomes $2n-1$. We can combine them and get an equation as

$$\begin{bmatrix} \mathbb{V}^1_z & -\mathbb{P}^1 \\ \mathbb{V}^2_z & \mathbb{P}^2 \end{bmatrix} \times \begin{bmatrix} \mathbb{F}^f_m \\ \mathbb{G}^f_m \end{bmatrix} = \begin{bmatrix} \mathbb{B} \\ 0 \end{bmatrix}, \tag{4-7}$$

based on which we can find solutions for vector $\mathbb{F}^f_m$ and $\mathbb{G}^f_m$ by constructing the left-hand side matrix with two-way marine data. $\mathbb{V}^1_z$ and $\mathbb{P}^1$ are the velocity and pressure matrices and $\mathbb{V}^2_z$ and $\mathbb{P}^2$ represent the time-reversal version of them.

Next, instead of constructing the matrices, we can also find expressions of $y_1 = A * x$ and $y_2 = A^T * x$ where the discrete convolution in time can be exactly computed with FFT. The computation time is much less than that of matrix construction method which will be demonstrated afterward.

From the mathematical point of view, the solution of equations with convolution and correlation relations is much easier to compute using FFT. Thus the expression in the function for computing y_1 is

$$\begin{bmatrix} real(ifft(fft(v_{z,new}) \cdot fft(f^f_{m,new}) - fft(p) \cdot fft(g^f_m))) \\ real(ifft((fft(v_{z,new}))^* \cdot fft(f^f_{m,new}) + (fft(p))^* \cdot fft(g^f_m))) \end{bmatrix}, \tag{4-8}$$

where $real(ifft())$ and $fft()$ are Matlab codes and they mean the real part of inverse Fourier transformed products. Then y_1 in the function called by LSQR can be computed by transforming the result of Eq. (4-8) back to time domain. Now that the computation of y_1 as a

result of $A * x$ is straightforward, the key point is then to find the solution of $A^T * x$. By observing the product of left-hand sides of Eq. (4-7) we can find that A^T can be written as

$$\begin{bmatrix} (\mathbb{V}_z^1)^T & (\mathbb{V}_z^2)^T \\ -(\mathbb{P}^1)^T & (\mathbb{P}^2)^T \end{bmatrix}. \tag{4-9}$$

Thus the expression in the function to compute y_2 is

$$\begin{bmatrix} flipud(real(ifft(fft(v_{z.new}) \cdot flipud(fft(f^f_{m,new})) + (fft(v_{z,new}))^* \cdot flipud(fft(g^f_m))))) \\ flipud(real(ifft(fft(-p) \cdot flipud(fft(f^f_{m,new})) + (fft(p))^* \cdot flipud(fft(g^f_m))))) \end{bmatrix}, \tag{4-10}$$

where $flipud()$ is also a Matlab command which means flip the vector up and down.

4-2 1D results of primaries at one-way traveltime

We first used a 1D model that consists of a free surface and 10 subsurface reflecting boundaries below the source level at $z_s = 10$ m and the receiver level at $z_r = 30$ m with the free surface above them at $z = 0$ m. The information of the layered model is given in Table 4-1.

Table 4-1: Density and velocity model and layer thickness.

Layer 1-6						
d(m)	175	217	199	285	211	275
$\rho(kg/m^3)$	1200	2250	1750	1430	1750	1930
c(m/s)	1500	1900	2100	1700	2100	2100
Layer 7-11						
d(m)	223	251	263	221	∞	
$\rho(kg/m^3)$	1700	2110	2110	2250	2300	
c(m/s)	2100	2300	2500	2750	2900	

The central frequency of source wavelet is 20 Hz. The focusing acoustic pressure and vertical particle velocity are computed as the output of the scheme presented in Figure 3-1 with focusing condition for flux-normalized wavefields. We solve the equations above by the LSQR method and imaged the upgoing primary reflections of all subsurface boundaries at the correct one-way traveltime following the same transmission response elimination scheme in [Slob et al., 2014].

Figure 4-1 and Figure 4-2 indicate the computed two-way acoustic pressure and vertical particle velocity as inputs of the revised Marchenko scheme. It is quite hard to identify each reflecting boundary from the input data. The outputs are corresponding pressure-related and velocity-related focusing wavefields. To check if we obtain the correct f^f and g^f under the flux-normalized focusing condition, we normalize them in terms of flux to get $p_A^{f,-}(z_r)$ which represents the reflection response. For each time instant in the data we compute $p_A^{f,-}(z_r)$ and we pick the value of $p_A^{f,-}(z_r)$ at time instant $t_d(z_i, z_r)$ and we store it. After we have solved the equations for all times we have a new trace that contains only the primary reflections. The free surface and internal multiples and the ghosts have been eliminated from the data and then we convolve the retrieved primary reflections with a 20 Hz Ricker wavelet. We give

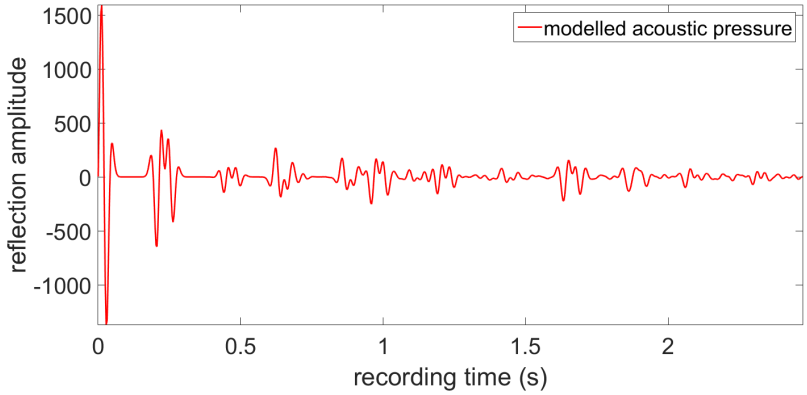

Figure 4-1: Modelled two-way acoustic pressure convolved with the 20 Hz wavelet

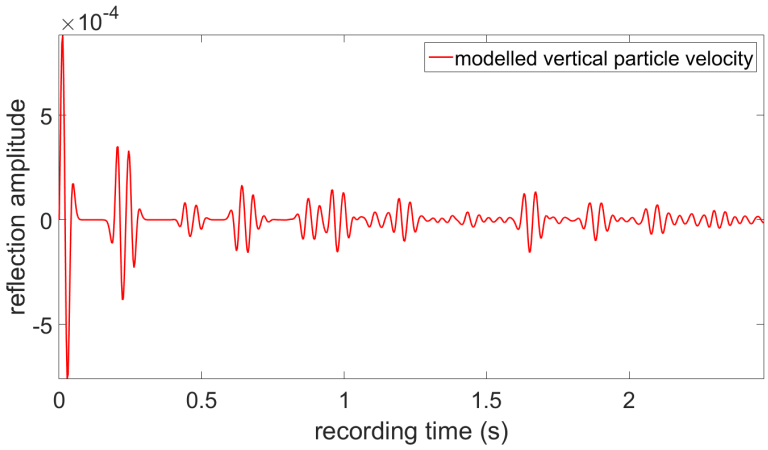

Figure 4-2: Modelled two-way vertical particle velocity convolved with the 20 Hz wavelet

one example of the upgoing focusing function in Figure 4-3. Equations Eq. (3-38) and Eq. (3-39) are solved for $t = 0.8125$ s explicitly as shown in Figure 4-3 and the value of computed $p_A^{f,-}(z_r)$ is taken at that time instant and stored in a new wavefield. In this example the time instant coincides with the one-way travel time of the 7^{th} subsurface reflector.

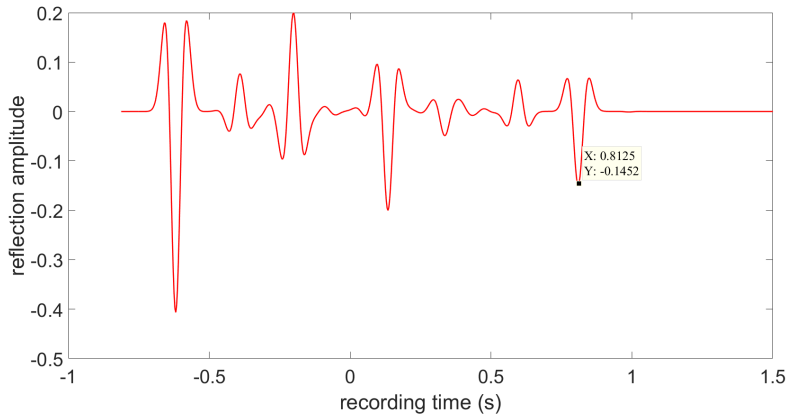

Figure 4-3: Upgoing focusing field at exactly the 7^{th} layer

In Figure 4-4 we plot the one-way retrieved primary reflections picked directly from all $p_A^{f,-}(z_r)$ (red dashed line) with the modelled primary reflections as reference where we can clearly see that at the 7^{th} layer the reflection amplitude coincides with that of Figure 4-3. Despite small discrepancies in the retrieved primary reflections, we can see a good match between retrieved primaries and modelled primaries both in phase and amplitude which illustrates the effectiveness of our scheme. Figure 4-5 and Figure 4-6 indicate the up- and downgoing Green's functions from the source to the focusing point. It can be clearly seen that before the first arrival, the Green's function is zero as we discussed before. We transform the focusing time to depth and the gather of Green's functions is shown in Figure 4-7 with corresponding focusing depths.

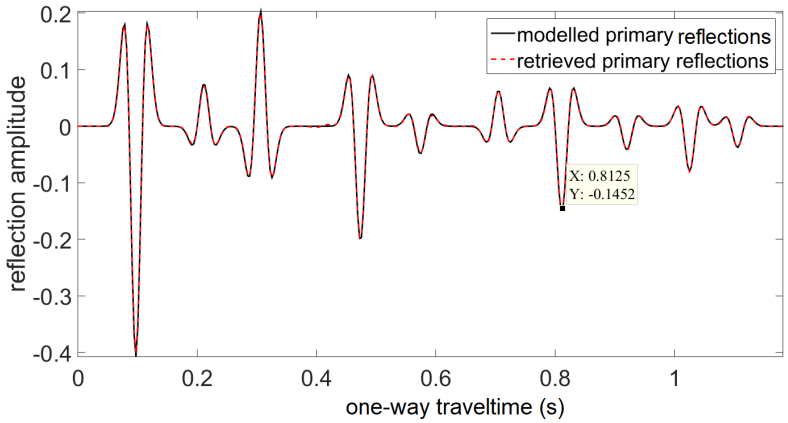

Figure 4-4: The obtained subsurface primaries (red dashed line) and the modelled reflectivity (black solid line) convolved with the 20 Hz Ricker wavelet as a function of one-way traveltime

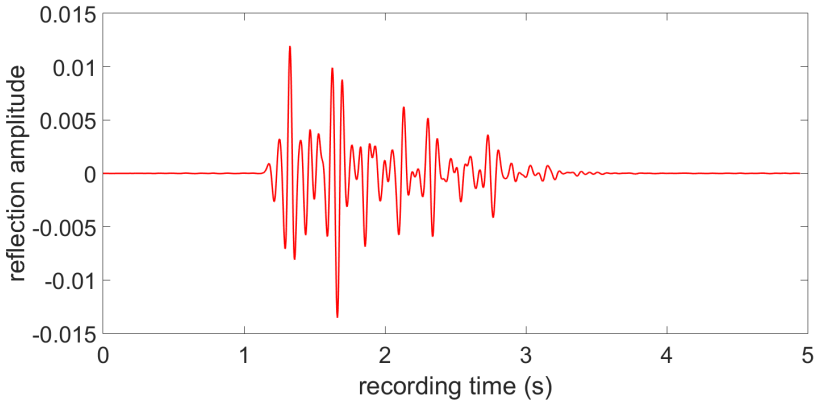

Figure 4-5: The obtained upgoing Green's function focusing at the 7^{th} layer

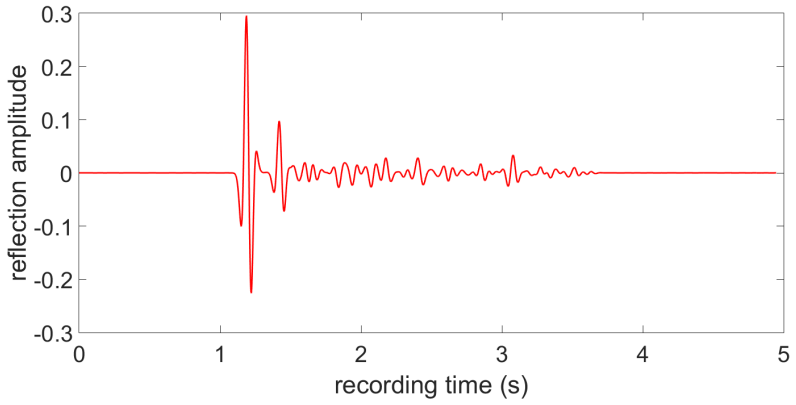

Figure 4-6: The obtained downgoing Green's function focusing at the 7^{th} layer

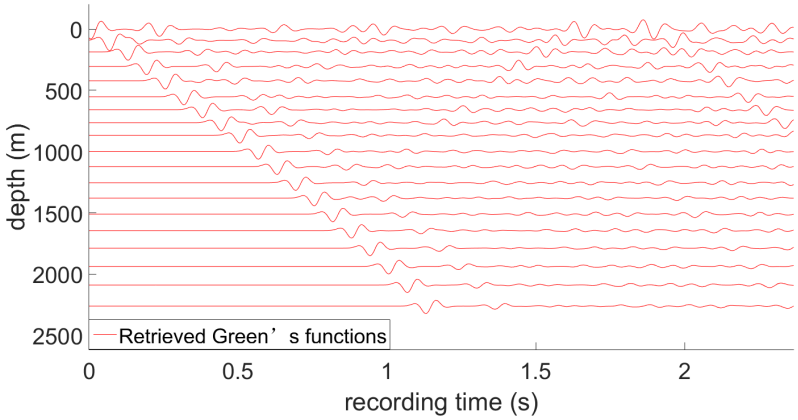

Figure 4-7: Gather of Green's functions at different focus depths

Moreover, the iteration needed for the last focusing depth level and the total computation time with matrix construction is 435 and 803.1s, respectively while for function handle method they become 346 and 38.5s. This shows that using function handle in LSQR is a better choice than using matrix.

Chapter 5

1D Model-Free Retrieval of Primaries From Marine Seismic Data

The Marchenko method is developed to compute the focusing functions from true acoustic pressure and vertical particle velocity. To retrieve the focusing functions an estimate of the first arrival of them is required. But in this chapter, we project the focusing functions back to the receiver level and this helps us to avoid the need of estimating direct arrival of downgoing focusing function for 1D situation. The resulting data fits better for velocity model building, which in turn can result in a better subsurface image than obtained from the measured data. Continuing with the Marchenko-type equations Eq. (3-38) and Eq. (3-39), we now project the focusing point back to the receiver level [van der Neut and Wapenaar, 2016]. The purpose of projection is to eliminate the need of the estimate of the direct downgoing focusing function $p^{f,+}_{A,d}(z_r, z_i, t)$ in Eq. (3-37) which occurs in the left-hand side of equation Eq. (3-38).
For the direct arrival part of the focusing function we have the relation given by [Wapenaar et al., 2014a]

$$\int_{t'=0}^{\infty} T^f_d(z_i, z_r, t') p^{f,+}_{A,d}(z_r, z_i, t - t') = \delta(t), \tag{5-1}$$

where $\delta(t)$ is a temporal delta function and T^f_d is the transmission response in terms of acoustic flux. Multiplying Eq. (3-28) with $\hat{T}^f_d(z_i, z_r)$ and Eq. (3-29) with $(\hat{T}^f_d(z_i, z_r))^*$ in frequency domain we obtain

$$\hat{u}^-(z_r, z_i, z_s) = -[\hat{w}^f(z_r, z_i, z_r)\hat{v}_z(z_r, z_s) - \hat{v}^f(z_r, z_i, z_r)\hat{p}(z_r, z_s)] + \hat{h}(z_r, z_s), \tag{5-2}$$

$$\hat{u}^+(z_r, z_i, z_s) = [(\hat{w}^f(z_r, z_i, z_r))^*\hat{v}_z(z_r, z_s) + (\hat{v}^f(z_r, z_i, z_r))^*\hat{p}(z_r, z_s)], \tag{5-3}$$

where

$$\hat{u}^-(z_r, z_i, z_s) = \hat{T}^f_d(z_i, z_r)\hat{p}^{f,-}(z_i, z_s), \tag{5-4}$$

$$\hat{u}^+(z_r, z_i, z_s) = (\hat{T}^f_d(z_i, z_r))^*\hat{p}^{f,+}(z_i, z_s), \tag{5-5}$$

$$\hat{w}^f(z_r, z_i, z_r) = \hat{T}^f_d(z_i, z_r)\hat{f}^f_m(z_r, z_i), \tag{5-6}$$

$$(\hat{w}^f(z_r,z_i,z_r))^* = (\hat{T}_d^f(z_i,z_r))^*(\hat{f}_m^f(z_r,z_i))^*, \tag{5-7}$$

$$\hat{v}^f(z_r,z_i,z_r) = \hat{T}_d^f(z_i,z_r)\hat{g}_m^f(z_r,z_i), \tag{5-8}$$

$$(\hat{v}^f(z_r,z_i,z_r))^* = (\hat{T}_d^f(z_i,z_r))^*(\hat{g}_m^f(z_r,z_i))^*, \tag{5-9}$$

$$\hat{h}(z_r,z_s) = 2\hat{T}_d^f(z_i,z_r)\hat{p}_{A,d}^{f,+}(z_r,z_i)\hat{p}^{f,-}(z_r,z_s) = 2\hat{p}^{f,-}(z_r,z_s), \tag{5-10}$$

Figure 5-1 shows how the projection works taking Eq. (5-4) as an example.

Eq. (5-2) and Eq. (5-3) can be written in the time domain as

$$\begin{aligned} &u^-(z_r,z_i.z_s;t) = h(z_r,z_s,t) \\ &-\int_{-\infty}^{t}[w^f(z_r,z_i,z_r;t')v_z(z_r,z_s,t-t') - v^f(z_r,z_i,z_r;t')p(z_r,z_s,t-t')]dt', \end{aligned} \tag{5-11}$$

$$\begin{aligned} &u^+(z_r,z_i.z_s;t) \\ &= \int_{-\infty}^{t}[w^f(z_r,z_i,z_r;-t')v_z(z_r,z_s,t-t') + v^f(z_r,z_i,z_r;-t')p(z_r,z_s,t-t')]dt'. \end{aligned} \tag{5-12}$$

Notice that $u^{\pm}(z_r,z_i,z_s;t)$, $w^f(z_r,z_i,z_r;t)$ and $v^f(z_r,z_i,z_r;t)$ depend on both the focusing point z_i which we focus at and the receiving point z_r which we project to. After projection, all fields are causal in time domain and $u^{\pm}(z_r,z_i,z_s;t)$ are the up- and downgoing parts of the projected wavefields. The time window of the wavefields is changed such that $u^{\pm}(z_r,z_i,z_s;t)$ starts at $t = t_2(z_r,z_i,z_s)$. We also have $w^f(z_r,z_i,z_r;t')$ and $v^f(z_r,z_i,z_r;t')$ as the projected focusing wavefields from the receiver level to the focusing surface and back to the receiver level for $0 < t \leq t_2'(z_r,z_i,z_r)$. For each focusing point we have a different two-way travel time $t_2(z_r,z_i,z_s)$ as the truncation window and the expressions in time domain after the normalization option mentioned above are given as

$$\begin{aligned} &\int_{t'=0}^{t_2}[v_z(z_r,z_s,t-t')w^f(z_r,z_i,z_r;t') - p(z_r,z_s,t-t')v^f(z_r,z_i,z_r;t')]dt' \\ &= h(z_r,z_s,t), \end{aligned} \tag{5-13}$$

$$\int_{-t_2}^{t'=0}[v_z(z_r,z_s,t+t')w^f(z_r,z_i,z_r;t') + p(z_r,z_s,t+t')v^f(z_r,z_i,z_r;t')]dt' = 0, \tag{5-14}$$

which enable us to determine the projected focusing functions using only the true marine data. For measured data, the right side of the time window should be adjusted to $t_2+\epsilon$ to account for the finite bandwidth. It is of interest to note that we don't need t_2. There always exists a depth level where we can focus to and project back from which coincides with the recording time t. This means that t_2 is not a necessary parameter and we use t. Consequently, we don't need a macro velocity model. Additionally, since the source wavelet doesn't appear in the coupled equations, we don't need source wavelet for the computation.

Then for each time instant in the data we solve equations Eq. (5-13) and Eq. (5-14) and compute the projected function $p_A^{fpro,-}(z_r)$. Then we take the value at that projected time instant and store it in a new wavefield which in the 1D situation only contains primary reflection response at two-way traveltime.

For Eq. (3-44) and Eq. (3-45) with velocity-normalized data in state B and Eq. (3-54) and Eq. (3-55) with pressure-normalized data in state B, we can also perform the same procedures as above but with different projection operator $\hat{T}_d^p(z_i,z_r)$ and $\hat{T}_d^v(z_i,z_r)$, respectively.

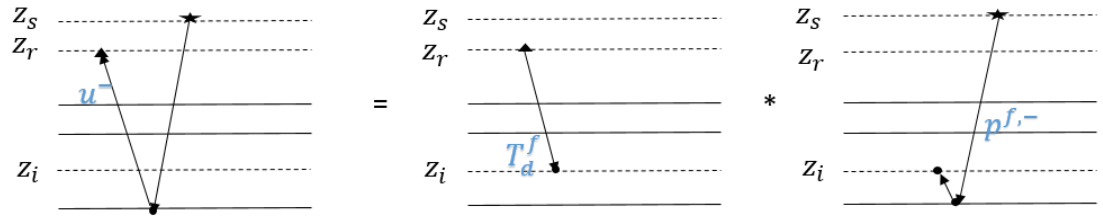

(a) Eq. (5-4) constructs the primaries which reflected from a layer deeper than the focusing level.

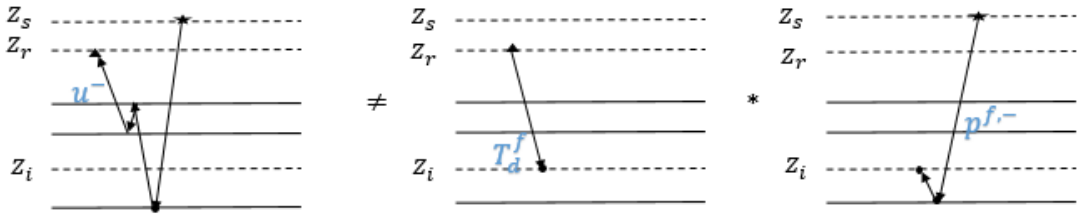

(b) Eq. (5-4) doesn't construct the internal multiples at the receiver side above z_i.

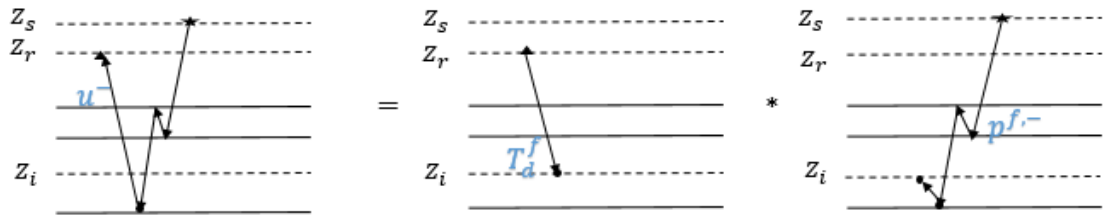

(c) Eq. (5-4) constructs the internal multiples at the source side above z_i.

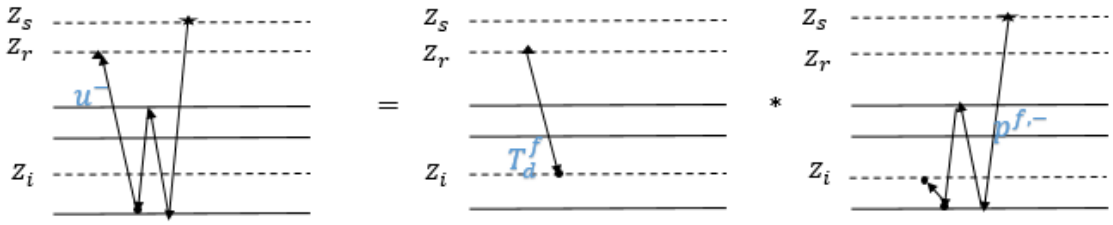

(d) Eq. (5-4) constructs the internal multiples at the source side above and below z_i

Figure 5-1: 1D sketch to illustrate Eq. (5-4)

5-1 1D Reflection of a plane wave at oblique incidence angle

The effect of the incident angle on local reflection coefficients can be characterized by slowness p, [Fryer, 1980]. And the one-way intercept time then becomes slowness-related given by $t_d(z_i, z_r, p) = \sum_{n=1}^{i} q_n(z_n - z_{n-1})$ where q_n is the vertical slowness in layer n [Slob et al., 2014]. Thus we can rewrite Eq. (5-13) and Eq. (5-14) in 1D version as

$$\begin{aligned}&\int_{t'=0}^{t_2} [v_z(z_r, z_s, t-t', p) w^f(z_r, z_i, z_r, t', p) - p(z_r, z_s, t-t', p) v^f(z_r, z_i, z_r, t', p)] dt' \\ &= h(z_r, z_s, t, p),\end{aligned} \tag{5-15}$$

$$\int_{-t_2}^{t'=0} [v_z(z_r, z_s, t+t', p) w^f(z_r, z_i, z_r, t', p) + p(z_r, z_s, t+t', p) v^f(z_r, z_i, z_r, t', p)] dt' = 0, \tag{5-16}$$

We use LSQR scheme to solve Eq. (5-15) and Eq. (5-16).

Chapter 6

Numerical Examples

In this chapter, we verify our scheme with the numerical examples for marine data with free-surface multiples, borehole data as well as zero and oblique angles of incidence. Since our scheme only deals with evanescent waves at the receiver level, we will solve the thin layer problem for data with oblique incidence angles by putting the receiver below the thin layer.

6-1 LSQR implementation

In matrix form, Eq. (5-13) and Eq. (5-14) can be written as

$$\begin{bmatrix} \frac{1}{2}v_{z,new}(j+1) & 0 & . & . & 0 \\ v_{z,new}(j+2) & \frac{1}{2}v_{z,new}(j+1) & 0 & . & 0 \\ . & . & . & 0 & 0 \\ . & . & . & . & 0 \\ v_{z,new}(j+2n) & . & . & v_{z,new}(j+2) & \frac{1}{2}v_{z,new}(j+1) \end{bmatrix} \times \begin{bmatrix} w^f_{new}(n,1) \\ . \\ . \\ w^f_{new}(n,2n-1) \\ w^f_{new}(n,2n-2) \end{bmatrix}$$

$$- \begin{bmatrix} \frac{1}{2}p(j+1) & 0 & . & . & 0 \\ p(j+2) & \frac{1}{2}p(j+1) & 0 & . & 0 \\ . & . & . & 0 & 0 \\ . & . & . & . & 0 \\ p(j+2n) & . & . & p(j+2) & \frac{1}{2}p(j+1) \end{bmatrix} \times \begin{bmatrix} v^f(n,1) \\ . \\ . \\ v^f(n,2n-1) \\ v^f(n,2n) \end{bmatrix}$$

$$= \begin{bmatrix} h(n,j+1) \\ . \\ . \\ h(n,j+2n-1) \\ h(n,j+2n) \end{bmatrix}, \tag{6-1}$$

$$\begin{bmatrix} 0 & 0 & . & 0 & \frac{1}{2}v_{z,new}(j+1) \\ 0 & . & 0 & v_{z,new}(j+1) & \frac{1}{2}v_{z,new}(j+2) \\ 0 & 0 & . & . & . \\ 0 & . & . & . & . \\ v_{z,new}(j+1) & v_{z,new}(j+2) & . & . & \frac{1}{2}v_{z,new}(j+2n) \end{bmatrix} \times \begin{bmatrix} w^f_{new}(n,1) \\ . \\ . \\ w^f_{new}(n,2n-1) \\ w^f_{new}(n,2n) \end{bmatrix}$$

$$+ \begin{bmatrix} 0 & 0 & . & 0 & \frac{1}{2}p(j+1) \\ 0 & . & 0 & p(j+1) & \frac{1}{2}p(j+2) \\ 0 & 0 & . & . & . \\ 0 & . & . & . & . \\ p(j+1) & p(j+2) & . & . & \frac{1}{2}p(j+2n) \end{bmatrix} \times \begin{bmatrix} v^f(n,1) \\ . \\ . \\ v^f(n,2n-1) \\ v^f(n,2n) \end{bmatrix}$$

$$= \begin{bmatrix} 0 \\ . \\ . \\ 0 \\ 0 \end{bmatrix}, \tag{6-2}$$

where $w^f_{new} = \frac{w^f}{10^6}$. Again from the above equations in matrix form, we can express y_1 is

$$\begin{bmatrix} real(ifft(\hat{v}_{z,new}\hat{w}^f_{new} - \hat{p}\hat{v}^f)) \\ real(ifft((\hat{v}_{z,new})^*\hat{w}^f_{new} + (\hat{p})^*\hat{v}^f)) \end{bmatrix}, \tag{6-3}$$

The expression for y_2 is then

$$\begin{bmatrix} flipud(real(ifft(\hat{v}_{z,new}flipud(\hat{w}^f_{new}) + (\hat{v}_{z,new})^* flipud(\hat{v}^f)))) \\ flipud(real(ifft(-\hat{p}flipud(\hat{w}^f_{new}) + (\hat{p})^* flipud(\hat{v}^f)))) \end{bmatrix}. \tag{6-4}$$

6-2 1D retrieval of two-way primaries with source and receiver below the free surface

We use the same 1D model given in Table 4-1 and the same source wavelet with a 20 Hz central frequency. Acoustic pressure and vertical particle velocity are the same as indicated in Figure 4-1 and Figure 4-2 are computed and v_z is multiplied with 10^6 again as the inputs of Eq. (5-13) and Eq. (5-14). We solve the equations using function handle in the LSQR method and retrieve the primary reflections of all subsurface boundaries at the correct two-way traveltime.

We show one example of the projected focusing function which is at the two-way traveltime from the receiver to the 7^{th} layer and back to the receiver in Figure 6-1. In Figure 6-2 we plot the two-way retrieved primary reflections picked from the value at each truncation time instant directly from all $p^{fpro,-}_A(z_r)$ (red dashed line) with the modelled primary reflections

as reference. Our scheme effectively retrieves the primaries at two-way travel time without the need of model information. We also used different models to test for further illustration of this scheme which are shown in Appendix B.

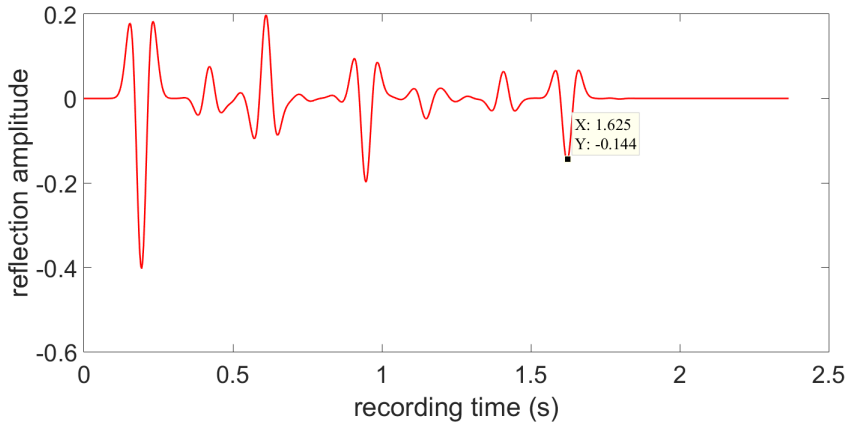

Figure 6-1: Upgoing focusing function exactly at the 7^{th} layer at two-way travel time

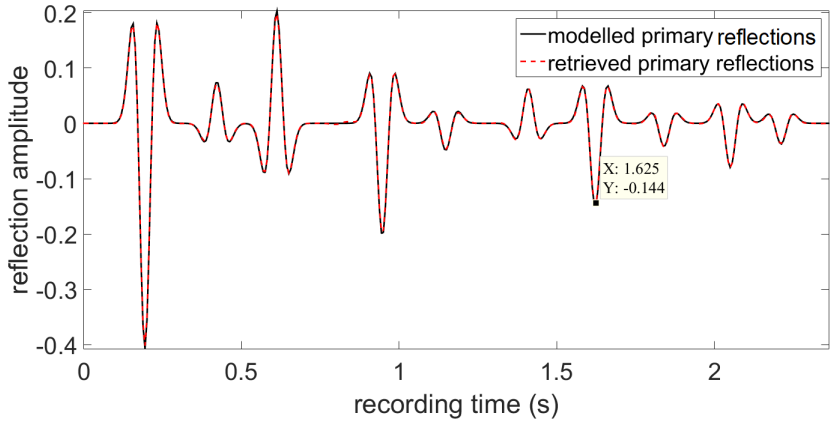

Figure 6-2: The obtained subsurface primaries (red dashed line) and the modelled reflectivity (black solid line) convolved with the 20 Hz Ricker wavelet as a function of two-way travel time

6-3 1D retrieval of two-way primaries for borehole data

Table 6-1: Density and velocity model and layer thickness.

Layer 1-6						
d(m)	175	352	399	285	211	275
$\rho(kg/m^3)$	1200	2250	1750	1430	1750	1930
c(m/s)	1500	1900	2100	1700	2100	2100
Layer 7-11						
d(m)	423	251	263	221	∞	
$\rho(kg/m^3)$	1700	2110	2110	2250	2300	
c(m/s)	2100	2300	2500	2750	2900	

We also tested the scheme for two sets of borehole data and we put the receiver below the 2^{nd} and the 7^{th} layer of model Table 6-1 at $z_r = 280$ m and $z_r = 1800$ m. We still put the source at $z_s = 10$ m and one can note that we only increase the depth of layers where we will put the receiver in order to avoid the thin layer errors caused by source wavelength of a 20 Hz Ricker wavelet. Figure 6-3 and Figure 6-4 indicate the input modelled borehole data with the receiver at $z_r = 280$ m where the unit direct arrival part of the impulsive source doesn't appear.

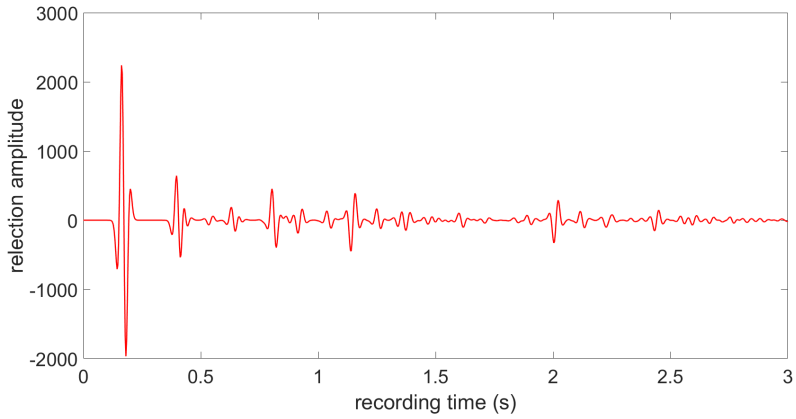

Figure 6-3: Modelled borehole acoustic pressure convolved with the 20 Hz wavelet with the receiver at $z_r = 280$ m

The upgoing focusing function is again shown in Figure 6-5 as an example where the two-way traveltime and the reflection amplitude are marked out. In Figure 6-6, we can only see 9 reflecting layers which are exactly what we want by putting the receiver at a depth of 280 m which means that all reflectors above the receiver are eliminated. Notice that in all numerical tests we include the free-surface. The solution of the reflection amplitude at the 7^{th} layer is still comparable to those of previous results with source and receiver just below the free surface.

The input data with the receiver at $z_r = 1800$ m are shown in Figure 6-7 and Figure 6-8. The multiples are much fewer than those with the receiver at $z_r = 280$ m. As can be seen in Figure 6-10, the primaries below the depth level are well recovered despite small errors among

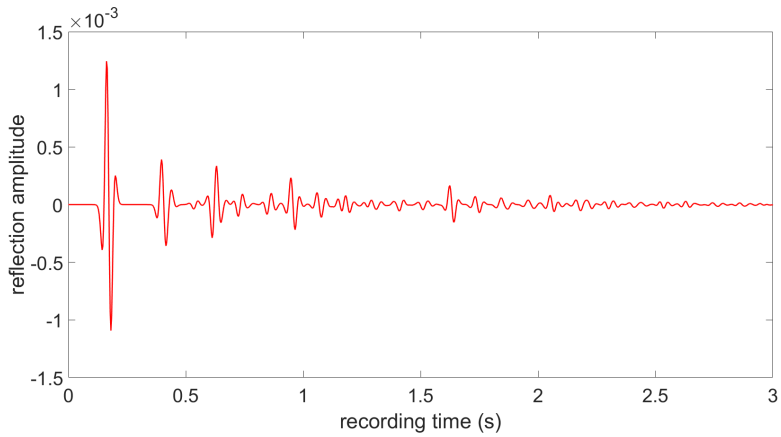

Figure 6-4: Modelled borehole vertical particle velocity convolved the 20 Hz wavelet with the receiver at $z_r = 280$ m

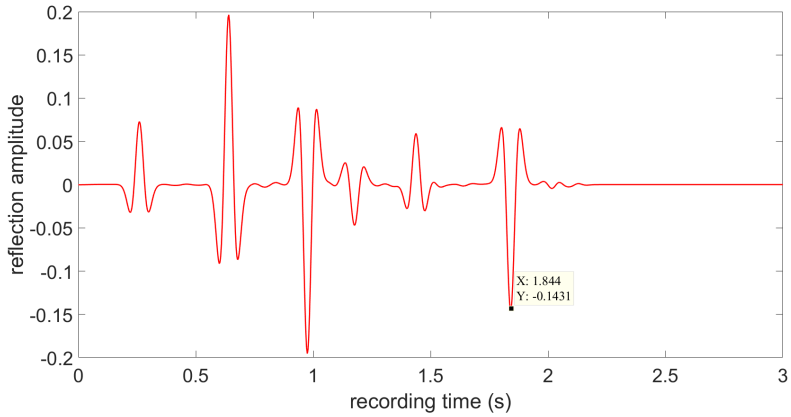

Figure 6-5: Upgoing focusing function exactly at the 7^{th} layer at two-way travel time with the receiver at $z_r = 280$ m

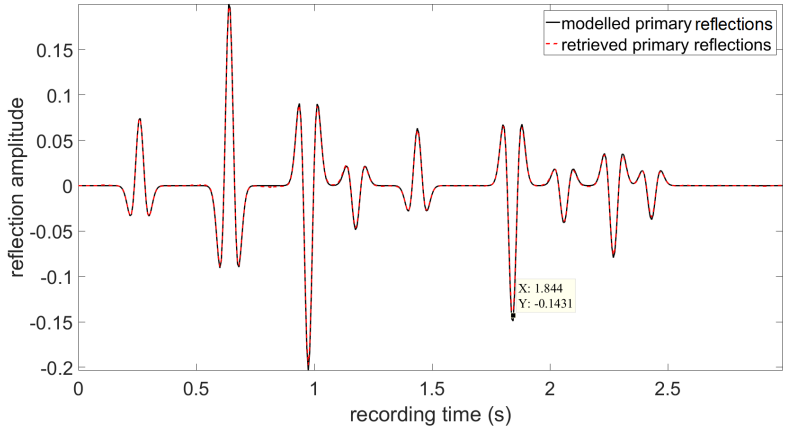

Figure 6-6: The obtained subsurface primaries (red dashed line) and the modelled reflectivity (black solid line) with the receiver at $z_r = 280$ m convolved with the 20 Hz Ricker wavelet as a function of two-way traveltime

the marked reflection coefficient of the 7^{th} layer in different schemes. It is worthy to notice that in Figure 6-9, there is only one reflecting event since the 7^{th} is the first layer below the receiver level.

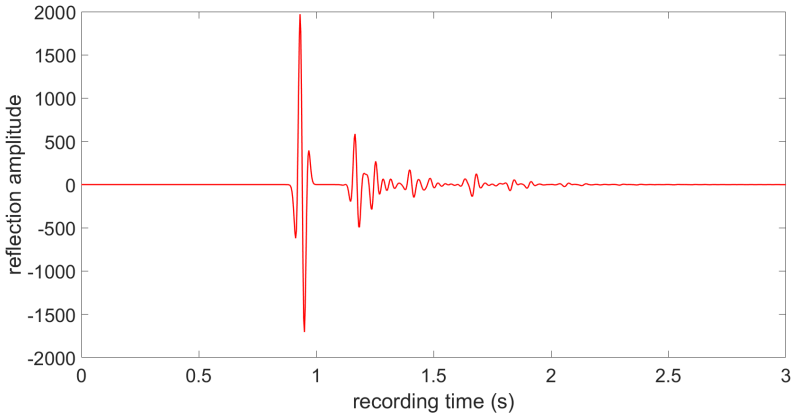

Figure 6-7: Modelled borehole acoustic pressure convolved with the 20 Hz wavelet with the receiver at $z_r = 1800$ m

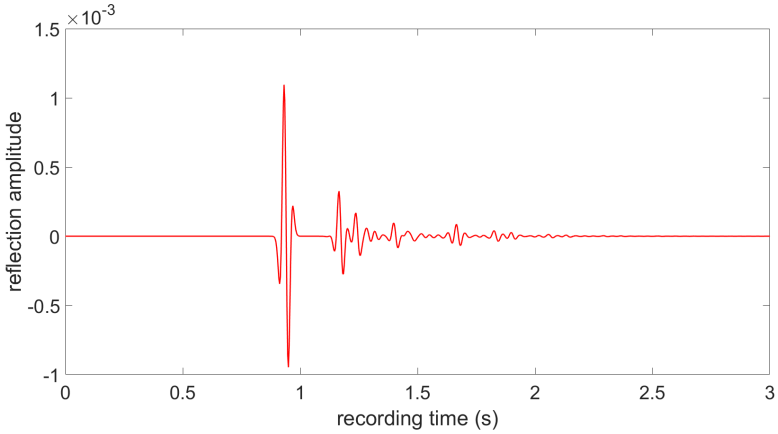

Figure 6-8: Modelled borehole vertical particle velocity convolved with the 20 Hz wavelet with the receiver at $z_r = 1800$ m

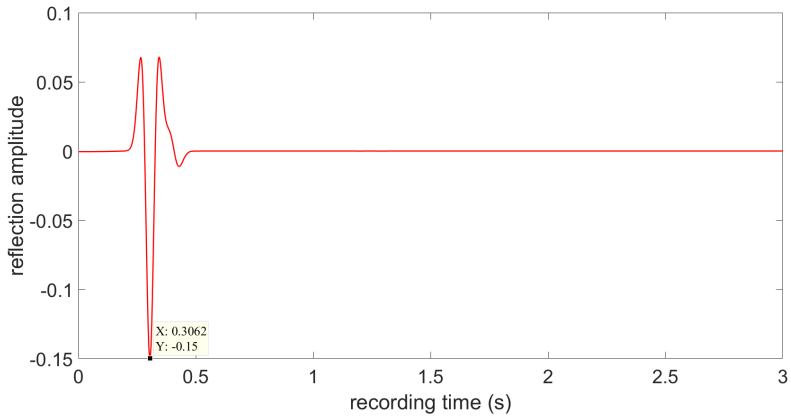

Figure 6-9: Projected focusing function exactly from the receiver to the 7^{th} layer and back to the receiver with the receiver at $z_r = 1800$ m

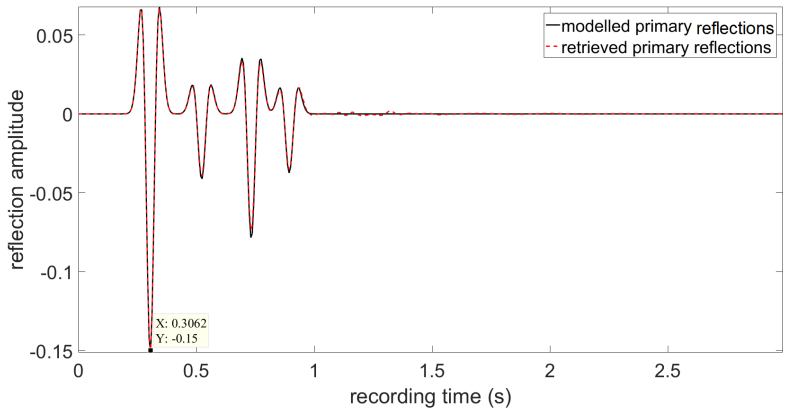

Figure 6-10: The obtained subsurface primaries (red dashed line) and the modelled reflectivity (black solid line) with the receiver at $z_r = 1800$ m convolved with Ricker wavelet as a function of two-way traveltime

6-4 1D retrieval of two-way primaries with oblique angles of incidence

In this section, we compare the results of normal numerical example where we put the source and receiver just below the free-surface and the numerical example of borehole data where we put the receiver below the 7^{th} layer to see how our scheme deal with the thin layer problem which causes the amplitude and phase inaccuracy of the recovery of the primaries below that thin layer when the incidence angle is greater than the critical angle. In both cases, we use the model shown in Table 6-2 where the thin layer is the 5^{th} reflecting layer and we set our incidence angle ranging from 0^o to 25^o. The output image will be a gather of 'traces' with

Table 6-2: Density and velocity model and layer thickness.

Layer 1-6						
d(m)	175	352	399	285	30	275
$\rho(kg/m^3)$	1200	2250	1750	1430	1750	1930
c(m/s)	1500	1900	2100	1700	3500	2100
Layer 7-11						
d(m)	423	251	263	221	∞	
$\rho(kg/m^3)$	1700	2110	2110	2250	2300	
c(m/s)	2100	2300	2500	2750	2900	

incident angle as x-axis and recording time as y-axis. We first put the source at $z_s = 10$ m and the receiver at $z_r = 30$ m which is the same configuration as that of previous examples with free-surface. The obtained image indicated gather of 'traces' of retrieved primaries as a function of two-way traveltime for different incident angles, see Figure 6-11. We can observe

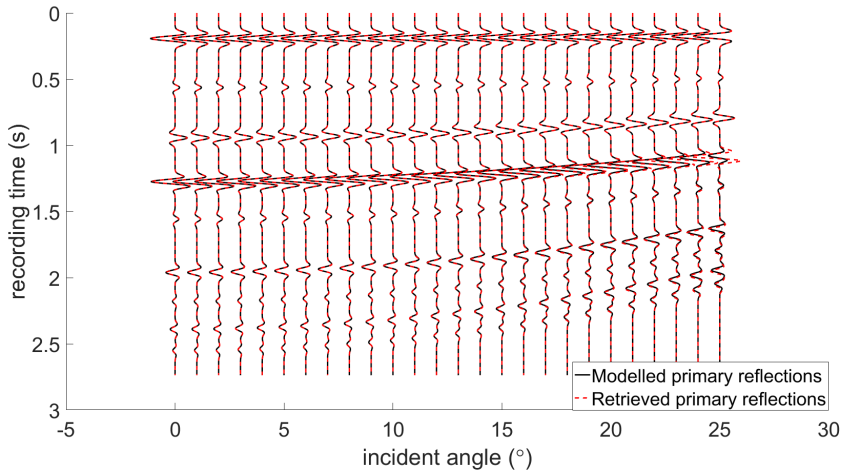

Figure 6-11: Gather of 'traces' with primaries as a function of two-way travel time with the source at $z_s = 10$ m and the receiver at $z_r = 30$ m

that as the incident angle increases, the arrival time of primaries decreases. For the 5^{th} layer, when the incident angle becomes larger than the critical angle, we can see the wrong recovery of both phase and amplitude of primaries for this layer and deeper layers which means that

Eq. (5-15) and Eq. (5-16) still don't deal with evanescent waves properly enough. Figure 6-12 indicates the explicit result at a 25^o incidence angle. The amplitude of the retrieved primary reflection of the 5^{th} layer is of great difference from the modelled one and moreover, it clearly shows that the phase and amplitude of the primary reflections of deeper layers are affected by the evanescent waves in the thin layer.

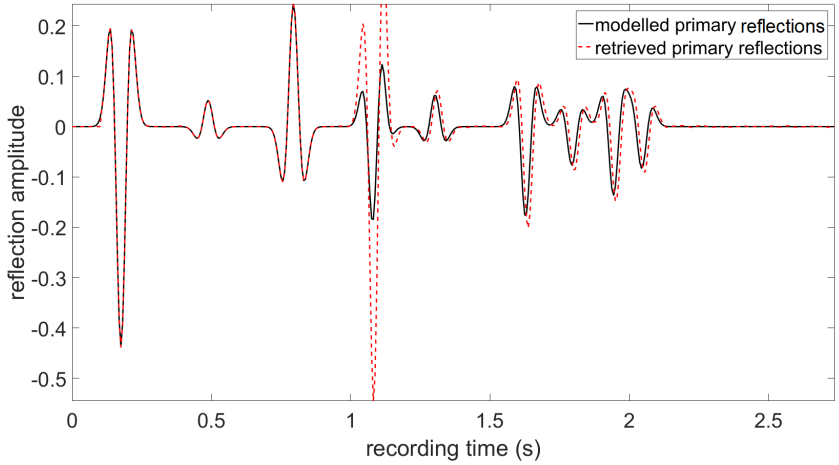

Figure 6-12: Modelled primaries (dark solid) and retrieved primaries (red dashed) at 25^o incidence angle with source at $z_s = 10$ m and receiver at $z_r = 30$ m

However, since our scheme works for borehole data, we can circumvent this thin layer problem by putting our receiver below the thin layer and above the target zone which we assume to be layer 7^{th} - 10^{th}. We keep the source position unchanged but we put the receiver at $z_r = 1700$ m. We can see good recovery of the primaries at different angles in Figure 6-13 and in Figure 6-14 the retrieved primaries of a 25^o incident field is also estimated much more accurate than that in Figure 6-12.

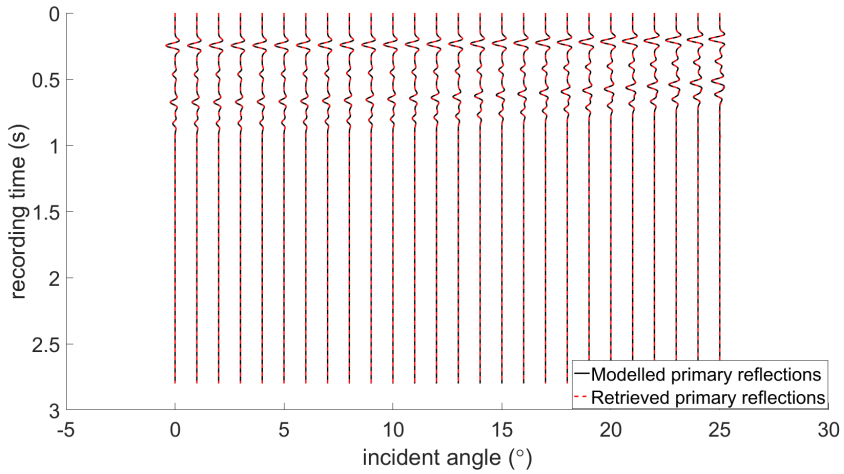

Figure 6-13: Gather of 'traces' with primaries as a function of two-way travel time with source at $z_s = 10$ m and receiver at $z_r = 1700$ m

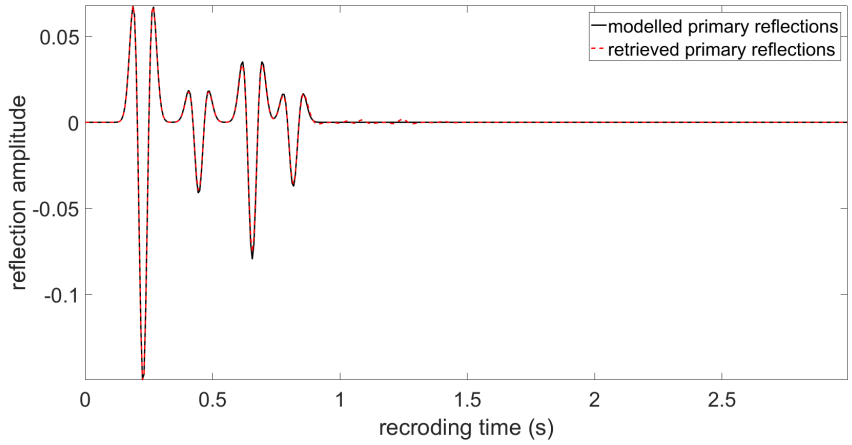

Figure 6-14: Modelled primaries (dark solid) and retrieved primaries (red dashed) at 25^o incidence angle with source at $z_s = 10$ m and receiver at $z_r = 1700$ m

Chapter 7

Conclusions and Further Research

7-1 Conclusions

We have formulated the reciprocity relations with the two-way wavefields at the receiver level and one-way wavefields at the focusing level. We show that with different choices of the focusing condition, the retrieved focusing wavefields were also of different relations with the reflection response. The scheme was tested and the retrieved results were both pressure-related and velocity-related focusing functions. To verify the results, we normalized those two focusing functions in terms of acoustic flux and obtained the flux-normalized upgoing focusing function which only included the primary reflections. It fitted the modelled reflections very well. The new scheme enables us to use the received data to retrieve the focusing functions in terms of pressure and vertical particle velocity, respectively. It simplifies the procedure of the whole Marchenko scheme.

Furthermore, we multiply both sides of the new Marchenko-type equations with the inverse of the direct arriving part of the downgoing focusing function so that the left-hand side fields and the focusing functions are projected to the receiver level. With this operator, we don't need an initial estimate of the direct arriving part of the downgoing focusing wavefields which requires the model information. From the standpoint of the 1D problem, this is a model-free scheme. We again tested it with a model containing free-surface and additionally, with borehole data as well as data with zero and oblique incidence of angles. In all cases, we successfully retrieved the primary reflections of the medium below the receivers.

It is also worth noticing that our solving method is different from the traditional method which builds up data matrices at each focusing point as the input of the LSQR function. We put the Marchenko-type equations in the function handle which we can call it with LSQR function at each focusing point. It reduces the computation time to less than 10% of that in the matrix inversion method.

7-2 Further Research

As to the possible further research considering this scheme, I believe that a 3D projection scheme with two-way wavefields retrieval needs to be developed.
Furthermore, algorithms on 2D numerical examples are suggested to be developed to test if our scheme works well for a very complex subsurface medium. The traditional iterative scheme doesn't work for this scheme since f_m and g_m are not connected with each other and a possible recommendation is to use LSQR approach to set up 2D Marchenko-type functions and its transpose version.
It is also worthy to do further study on possible applications of this scheme like medical imaging, GPR detection and so on.

Bibliography

[Broggini et al., 2012] Broggini, F., Snieder, R., and Wapenaar, K. (2012). Focusing the wavefield inside an unknown 1d medium: Beyond seismic interferometry. *Geophysics*, 77(5):A25–A28.

[Broggini et al., 2014] Broggini, F., Snieder, R., and Wapenaar, K. (2014). Data-driven wavefield focusing and imaging with multidimensional deconvolution: Numerical examples for reflection data with internal multiples. *Geophysics*, 79(3):WA107–WA115.

[Claerbout, 1985] Claerbout, J. (1985). *Fundamentals of Geophysics Data Processing*. Blackwell Scientific.

[Cypriano et al., 2015] Cypriano, L., Marpeau*, F., Brasil, R., Welter, G., Prigent, H., Douma, H., Velasques, M., Boechat, J., de Carvalho, P., Guerra, C., Theodoro, C., Martini, A., and Cruz, J. N. (2015). The impact of inter-bed multiple attenuation on the imaging of pre-salt targets in the santos basin off-shore brazil. *77th EAGE Conference and Exhibition*.

[Fishman, 1987] Fishman, L. (1987). Factorization and path integration of the Helmholtz equation: Numerical algorithms. *The Journal of the Acoustical Society of America*, 81:1355.

[Fishman, 1993] Fishman, L. (1993). One-way propagation methods in direct and inverse scalar wave propagation modeling. *Radio Science - RADIO SCI*, 28:865–876.

[Fomel, 2009] Fomel, S. (2009). Adaptive multiple subtraction using regularized nonstationary regression. *Geophysics*, 74(1):V25–V33.

[Fryer, 1980] Fryer, G. J. (1980). A slowness approach to the reflectivity method of seismogram synthesis. *Geophysical Journal International*, 63:747–758.

[Jakubowicz, 2005] Jakubowicz, H. (2005). Wave equation prediction and removal of interbed multiples. *SEG Technical Program Expanded Abstracts 1998*, pages 1527–1530.

[Kelamis et al., 2006] Kelamis, P. G., Zhu, W., Rufaii, K. O., and Luo, Y. (2006). Land multiple attenuation the future is bright. *SEG Technical Program Expanded Abstracts 2006*, pages 2699–2703.

[King et al., 2013] King, S., Dyer, R., and O'Neill, P. (2013). Data-driven internal multiple attenuation: Theory and examples. *SEG Technical Program Expanded Abstracts 2013*, pages 4089–4093.

[Matson et al., 1999] Matson, K., Corrigan, D., Weglein, A., Young, C., and Carvalho, P. (1999). *Inverse scattering internal multiple attenuation: Results from complex synthetic and field data examples*, pages 1060–1063. SEG Technical Program Expanded Abstracts 1999.

[P. Corones et al., 1983] P. Corones, J., E. Davison, M., and J. Krueger, R. (1983). Direct and inverse scattering in the time domain via invariant imbedding equations. *Journal of The Acoustical Society of America - J ACOUST SOC AMER*, 74:1535–1541.

[Ravasi, 2017] Ravasi, M. (2017). Rayleigh-Marchenko redatuming for target-oriented, true-amplitude imaging. *Geophysics*, 82(6):S439S452.

[Rose, 2002] Rose, J. H. (2002). 'Single-sided' autofocusing of sound in layered materials. *Inverse Problems*, 18(6):1923.

[Singh et al., 2015] Singh, S., Snieder, R., Behura, J., van der Neut, J., Wapenaar, K., and Slob, E. (2015). Marchenko imaging: Imaging with primaries, internal multiples, and free-surface multiples. *Geophysics*, 80(5):S165–S174.

[Singh et al., 2017] Singh, S., Snieder, R., van der Neut, J., Thorbecke, J., Slob, E., and Wapenaar, K. (2017). Accounting for free-surface multiples in Marchenko imaging. *Geophysics*, 82(1):R19–R30.

[Slob and Wapenaar, 2017] Slob, E. and Wapenaar, K. (2017). Theory for Marchenko imaging of marine seismic data with free surface multiple elimination. *79th EAGE Conference & Exhibition*.

[Slob et al., 2014] Slob, E., Wapenaar, K., Broggini, F., and Snieder, R. (2014). Seismic reflector imaging using internal multiples with Marchenko-type equations. *Geophysics*, 79(2):S63S76.

[T. de Hoop, 1995] T. de Hoop, A. (1995). *Handbook of Radiation and Scattering of Waves: Acoustic Waves in Fluids, Elastic Waves in Solids, Electromagnetic Waves*. Academic Press.

[Thorbecke et al., 2017] Thorbecke, J., Slob, E., Brackenhoff, J., van der Neut, J., and Wapenaar, K. (2017). Implementation of the Marchenko method. *Geophysics*, 82:1–56.

[Ursin, 1983] Ursin, B. (1983). Review of elastic and electromagnetic wave propagation in layered media. *Geophysics*, 48:1063–1081.

[van der Neut and Wapenaar, 2016] van der Neut, J. and Wapenaar, K. (2016). Adaptive overburden elimination with the multidimensional marchenko equation. *Geophysics*, 81(5):T265–T284.

[Wapenaar, 1998] Wapenaar, C. (1998). Reciprocity properties of one-way propagators. *Geophysics*, 63.

[Wapenaar and Berkhout, 1989] Wapenaar, C. and Berkhout, A. (1989). *Elastic wave field extrapolation: Redatuming of single- and multi- component seismic data, ser.* Advances in Exploration Geophysics. El-sevier Science Publishers.

[Wapenaar et al., 2001] Wapenaar, C., Dillen, M. P., and Fokkema, J. (2001). Reciprocity theorems for electromagnetic or acoustic one-way wave fields in dissipative inhomogeneous media. *Radio Science - RADIO SCI*, 36:851–863.

[Wapenaar et al., 2013] Wapenaar, K., Broggini, F., Slob, E., and Snieder, R. (2013). Three-dimensional single-sided Marchenko inverse scattering, data-driven focusing, Green's function retrieval, and their mutual relations. *Phys. Rev. Lett.*, 110:084301.

[Wapenaar et al., 2014a] Wapenaar, K., Thorbecke, J., van der Neut, J., Broggini, F., Slob, E., and Snieder, R. (2014a). Green's function retrieval from reflection data, in absence of a receiver at the virtual source position. *The Journal of the Acoustical Society of America*, 135(5):2847–2861.

[Wapenaar et al., 2014b] Wapenaar, K., Thorbecke, J., van der Neut, J., Broggini, F., Slob, E., and Snieder, R. (2014b). Marchenko imaging. *Geophysics*, 79(3):WA39–WA57.

[Weglein et al., 1997] Weglein, A. B., Gasparotto, F. A., Carvalho, P. M., and Stolt, R. H. (1997). An inverse-scattering series method for attenuating multiples in seismic reflection data. *Geophysics*, 62(6):1975–1989.

[Zhang et al., 2018a] Zhang, L., Slob, E., van der Neut, J., and Wapenaar, K. (2018a). Artefact-free reverse-time migration. *Geophysics*, pages 1–20.

[Zhang et al., 2018b] Zhang, L., Thorbecke, J., Wapenaar, K., and Slob, E. (2018b). Transmission compensated primary reflection retrieval in data domain and consequences for imaging. *Submitted to Geophysics*.

Appendix A

Evanescent Plane Waves Decomposition

A-1 Evanescent wave

The incidence of seismic plane waves on an interface follows Snell's law indicated in Figure A-1 considering a 1D plane wave. However, the Snell's law doesn't actually have solutions for

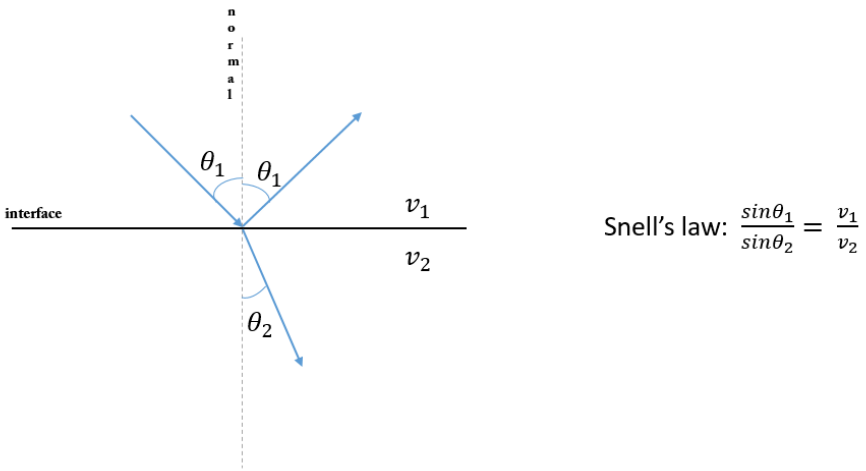

Figure A-1: Illustration of Snell's law

every possible combination of v_1, v_2 θ_1 and θ_2. In fact if we solve for θ_2 we ge the following

$$\theta_2 = arcsin(\frac{v_1}{v_2} sin\theta_1), \tag{A-1}$$

where if $\frac{v_1}{v_2} sin\theta_1$ we have a problem. We can not get to a solution for θ_2. In this case, we can flip that around into a condition on θ_1 that $\theta_1 > arcsin(\frac{v_2}{v_1})$. The direct message from this

condition is that the waves have to be going from some material of great wave propagation velocity to some material of less propagation velocity. However, this is quite opposite to the real situation of the subsurface. Alternatively, we can constraint the incident angle with the critical angle $\theta_c = arcsin(\frac{v_2}{v_1})$. If $\theta_1 > \theta_c$, we can't get the solution for the transmitted angle θ_2. Does that just mean that there is no transmitted wave and we get 100% internal reflection? The answer is no in the mathematical point of view. To explain this, we take the propagation of 3D homogeneous plane wave as an example [Wapenaar and Berkhout, 1989]. Except for θ, we need to introduce another angle α, see Figure A-2. The slowness vector

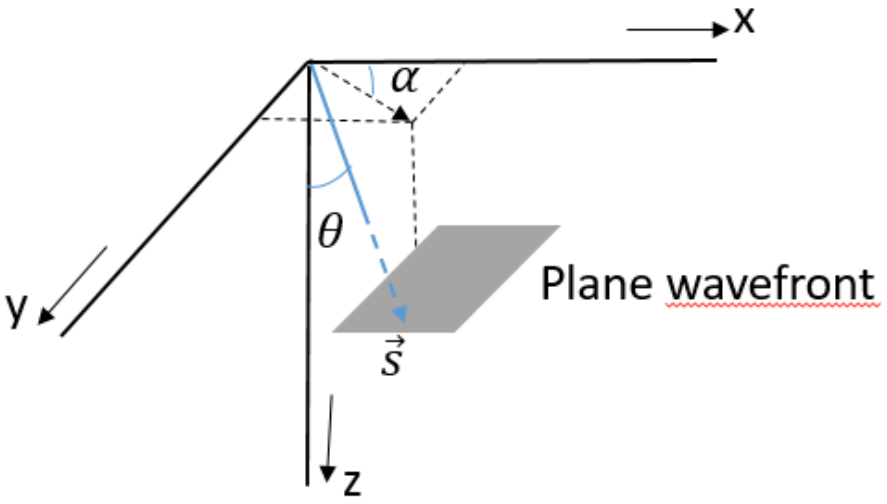

Figure A-2: 3D homogeneous plane wave incidence. $\vec{s}$ is the slowness vector with $\vec{s} - \frac{1}{\vec{c}}$ which can be decomposed into three directional components.

shown in Figure A-2 can be written according to

$$\vec{s} = |\vec{s}| \begin{bmatrix} sin\theta cos\alpha \\ sin\theta cos\alpha \\ cos\theta \end{bmatrix} = \begin{bmatrix} s_x \\ s_y \\ s_z \end{bmatrix}, \tag{A-2}$$

where $s_z^2 = |\vec{s}|^2 - s_x^2 - s_y^2$. When the incident angle is larger than the critical angle, we have $s_x^2 - s_y^2 > |\vec{s}|^2$ and this results in the fact that $s_z^2 < 0$. In this case, s_z is an imaginary value and we define the plane waves as evanescent waves. The expression of plane waves can then be written within a complex notation as

$$\hat{p}(x, y, z, t) = \hat{p_0} e^{j\omega(t - s_x x - s_y y - s_z z)}, \tag{A-3}$$

where $s_z = \sqrt{|\vec{s}|^2 - s_x^2 - s_y^2}$ for propagating waves and $s_z = -j\sqrt{s_x^2 + s_y^2 - |\vec{s}|^2}$ for evanescent waves. In frequency and wavenumber domain, Eq. (A-3) becomes

$$\tilde{p}(k_x, k_y, z, \omega) = \int_{-\infty}^{\infty} \int_{-\infty}^{\infty} \int_{-\infty}^{\infty} \hat{p}(x, y, z, t) e^{-j(\omega t - k_x x - k_y y)} dt dx dy, \tag{A-4}$$

where $k_x = \omega s_x$ and $k_y = \omega s_y$ and they are called horizontal wavenumbers. With (A-4), the propagation of acoustic can be defined as

$$\tilde{p}(k_x, k_y, z, t) = \tilde{p}_0 e^{j(\omega t - k_x x - k_y y - k_z z)}, \tag{A-5}$$

where $k_z = \sqrt{(\omega|\vec{s}|)^2 - k_x^2 - k_y^2}$ for propagating waves and $k_z = -j\sqrt{k_x^2 + k_y^2 - (\omega|\vec{s}|)^2}$ for evanescent waves. We decompose the acoustic pressure as $\tilde{p}^+ + \tilde{p}^-$ and obtain the following relation

$$\tilde{p}^{\pm}(k_x, k_y, z, t) = \tilde{p}_0^{\pm} e^{j(\omega t - k_x x - k_y y \mp k_z z)}. \tag{A-6}$$

In the source-free medium, the vertical derivatives of up- and downgoing acoustic pressure are

$$\frac{\partial \tilde{p}\pm}{\partial z} = \mp j k_z \tilde{p}\pm. \tag{A-7}$$

This gives us a general solution of one-way wavefields

$$\tilde{p}\pm(k_x, k_y, z, \omega) = e^{\mp j k_z (z - z_0)} \tilde{p}_0\pm(k_x, k_y, z_0, \omega). \tag{A-8}$$

Then we define two forward operators $\tilde{w}^{\pm}$ to describe the propagation of evanescent waves and we have $\tilde{W}^{\pm} = e^{\mp j k_z \Delta z}$ the absolute value of which is illustrated in Figure A-3. The evanescent waves are pointed out with arrows which exponentially decreases with $\sqrt{k_x^2 + k_y^2}$.

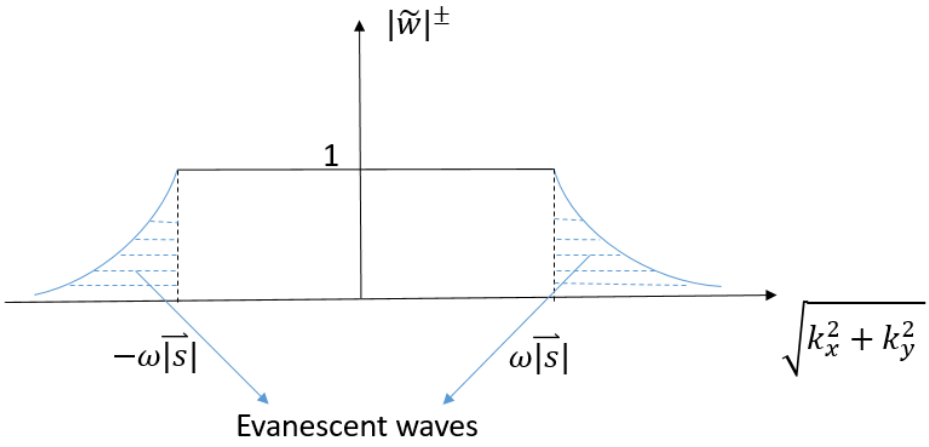

Figure A-3: 3D homogeneous plane wave incidence. $\vec{s}$ is the slowness vector with $\vec{s} - \frac{1}{\tilde{c}}$ which can be decomposed into three directional components.

A-2 One-way reciprocity theorem of correlation type

Since evanescent waves exponentially decreases as they go deeper, we can say that the forward operators $\tilde{W}^{\pm}$ is stable. However, if we define a backward propagator which is called $\tilde{F}^{\pm}$, the relations describing wave propagation becomes

$$\tilde{p}\pm(k_x, k_y, z_0, \omega) = \tilde{F}^{\pm} \tilde{p}_0\pm(k_x, k_y, z, \omega). \tag{A-9}$$

What we can learn by combining Eq. (A-8) and Eq. (A-9) is that $\tilde{W}^{\pm}(z_0, z_1) \cdot \tilde{F}^{\pm}(z_1, z_0) = 1$. But if we take this relation to solve for $\tilde{F}^{\pm}(z_1, z_0)$ we will find that it exponentially increases at the part evanescent waves. Therefore, we can take this solution as our backward propagator which will definite become unstable when it comes to evanescent waves. Instead of taking $\frac{1}{\tilde{W}^{\pm}(z_0,z_1)}$, we choose $[\tilde{W}^{\pm}(z_0, z_1)]^*$ and alternatively, $[\tilde{W}^{\mp}(z_1, z_0)]^*$ to approximate $\tilde{F}^{\pm}(z_1, z_0)$. In the correlation typed one-way reciprocity theorem, we use $\approx$ to connection both sides of equations since $[]^*$ doesn't represent the inverse of exact evanescent waves. That's why we need to make the assumption that the evanescent waves need to be ignored in the one-way reciprocity of correlation type.

Appendix B

Numerical Results with different models

Table B-1: Density and velocity model and layer thickness.

Layer 1-6						
d(m)	155	97	299	85	311	175
$\rho(kg/m^3)$	1900	1250	1940	2630	1570	1830
c(m/s)	1700	1750	2000	1800	1900	1700
Layer 7-11						
d(m)	123	174	287	295	∞	
$\rho(kg/m^3)$	1700	2110	2110	2250	2300	
c(m/s)	2200	2400	2500	2700	2800	

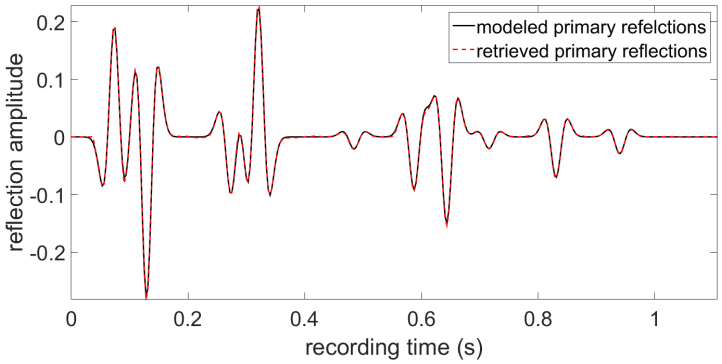

Figure B-1: The obtained subsurface primaries (red dashed line) and the model reflectivity (black solid line) convolved with Ricker wavelet as a function of one-way traveltime for model in Table B-1

Table B-2: Density and velocity model and layer thickness.

Layer 1-6						
d(m)	175	192	209	256	302	225
$\rho(kg/m^3)$	1520	2150	1560	1710	1640	1730
c(m/s)	1500	1640	1900	1800	2000	2050
Layer 7-11						
d(m)	123	201	313	178	∞	
$\rho(kg/m^3)$	1740	2110	2110	2250	2300	
c(m/s)	2200	2140	2440	2650	2890	

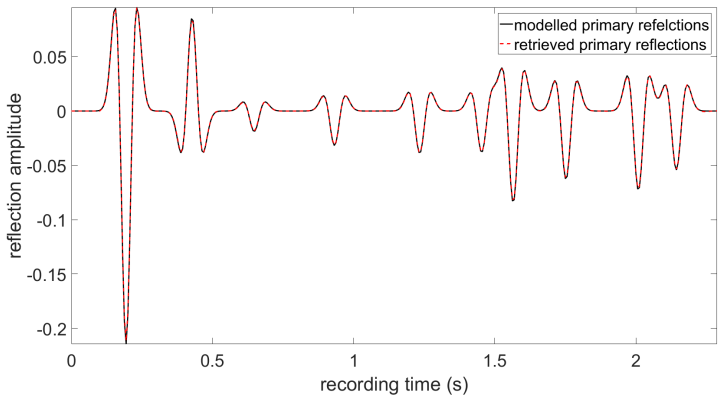

Figure B-2: The obtained subsurface primaries (red dashed line) and the model reflectivity (black solid line) convolved with Ricker wavelet as a function of one-way traveltime for model in Table B-2